DePhine – The Deimos and Phobos Interior Explorer

Jürgen Oberst
German Aerospace Center (DLR), Institute of Planetary Research *, Berlin, Germany and Technical University Berlin, Institute of Geodesy and Geoinformation Science, Berlin, Germany

Kai Wickhusen, Konrad Willner, Klaus Gwinner
German Aerospace Center (DLR), Institute of Planetary Research, Rutherfordstr. 2, D-12489 Berlin, Germany

Sofya Spiridonova and Ralph Kahle
German Aerospace Center (DLR), Space Flight Technology, D-82234 Oberpfaffenhofen-Wessling, Germany

Andrew Coates

MSSL-UCL Mullard Space Science, Laboratory University College London Holmbury St Mary Dorking, Surrey, RH5 6NT, UK

Alain Herique
Univ. Grenoble Alpes, CNRS, IPAG, F-38000 Grenoble, France

Dirk Plettemeier
Technische Universität Dresden, Professur für Hochfrequenztechnik, Würzburger Str. 35, D-01187 Dresden, Germany

Marina Díaz Michelena
Space Programs and Space Sciences Department, Instituto Nacional de Tecnica Aeroespacial (INTA), Madrid 28850, Spain

Alexander Zakharov
Space Research Institute of the Russian Academy of Sciences, Profsoyuznaya ul. 84/32, 117997 Moscow, Russia

Yoshifumi Futaana
Swedish Institute of Space Physics, Box 812, SE-98128 Kiruna, Sweden

Martin Pätzold
Rheinisches Institut für Umweltforschung,Universität zu Köln,D-50931 Köln Germany

Pascal Rosenblatt
Royal Observatory of Belgium (ROB), Av. Circulaire 3, B-1180 Uccle, Belgium

David J. Lawrence
Space Department, The Johns Hopkins University, Applied Physics Laboratory, 11100 Johns Hopkins Road, Laurel, MD 20723, USA

Valery Lainey
Institut de Mécanique Céleste et de Calcul de Ephémérides, Observatoire de Paris, UMR 8028 du CNRS, UPMC, 77 Av. Denfert-Rochereau

Alison Gibbings and Ingo Gerth
OHB System AG, Universitätsallee 27-29, D-28359 Bremen, Germany

*) Corresponding Author:

Jürgen Oberst
German Aerospace Center (DLR), Institute of Planetary Research, Rutherfordstr. 2, D-12489 Berlin, Germany

Juergen.Oberst@dlr.de, +49 30 67055-336

Abstract

DePhine – Deimos and Phobos Interior Explorer – is proposed in the context of ESA's Cosmic Vision program, for launch in 2030. The mission will explore the origin and the evolution of the two Martian satellites, by focusing on their interior structures and diversity, by addressing the following open questions: Are Phobos and Deimos true siblings, originating from the same source and sharing the same formation scenario? Are the satellites rubble piles or solid bodies? Do they possess hidden deposits of water ice in their interiors? The DePhine spacecraft will be inserted into Mars transfer and will initially enter a Deimos quasi-satellite orbit to carry out a comprehensive global mapping. The goal is to obtain physical parameters and remote sensing data for Deimos comparable to data expected to be available for Phobos at the time of the DePhine mission for comparative studies. As a highlight of the mission, close flybys will be performed at low velocities, which will increase data integration times, enhance the signal strength and data resolution. 10 – 20 flyby sequences, including polar passes, will result in a dense global grid of observation tracks. The spacecraft orbit will then be changed into a Phobos resonance orbit to carry out multiple close flybys and to perform similar remote sensing as for Deimos. The spacecraft will carry a suite of remote sensing instruments, including a camera system, a radio science experiment, a high-frequency radar, a magnetometer, and a Gamma Ray / Neutron Detector. A steerable antenna will allow simultaneous radio tracking and remote sensing observations (which is technically not possible for Mars Express). Additional instrumentation, e.g. a dust detector and a solar wind sensor, will address

further science goals of the mission. If Ariane 6-2 and higher lift performance are available for launch (the baseline mission assumes a launch on a Soyuz Fregat), we expect to have greater spacecraft mobility and possibly added payloads.

1 Introduction

DePhine – the Deimos and Phobos Interior Explorer – has been proposed as M-class mission in the context of ESA's Cosmic Vision program, with the spacecraft projected for launch in 2030. The mission will explore the origin and the evolution of the Martian natural satellites and will also contribute to the general questions of planetary formation and the workings of the solar system. Up to the present day, the origins of Phobos and Deimos are uncertain. They may have co-accreted with the parent planet (Safronov and Vitjazev, 1986), or formed from Martian impact basin ejecta (Citron et al., 2015; Craddock, 2011; Rosenblatt and Charnoz, 2012; Rosenblatt et al., 2016). Alternatively, they may represent captured primitive asteroids or comets (Burns, 1992). Clues on the origins of the satellites may come from comparative studies of whether Phobos and Deimos are true siblings, originate from the same source and share the same formation scenario and history. Other clues may come from investigations of the interior structures of the satellites, e.g., to resolve whether the satellites are rubble piles or solid bodies, or whether they possess hidden deposits of water ice in their interiors.

The DePhine spacecraft will initially enter a quasi-satellite orbit of Deimos to carry out a comprehensive remote-sensing campaign. The spacecraft will then move into an orbit in resonance with Phobos to carry out multiple flybys and to perform remote sensing experiments similar to those for Deimos for comparative studies. The spacecraft will carry a suite of remote sensing instruments, including a camera system, a radio science experiment, a high-frequency radar, a magnetometer, and a Gamma-Ray/Neutron spectrometer (GRNS). In addition, the spacecraft will be equipped with dust detectors and a solar wind sensor.

2 Science Cases

The mission aims at investigations of the origins of the two satellites, by an in-depth study of the diversity of Deimos and Phobos. Quite naturally, the mission will first focus on Deimos, to obtain its physical parameters and characteristics, at a level comparable to information already available for Phobos. In particular, we wish to determine the properties of the Deimos soil to enable comparisons with Phobos samples, expected to be available at the time of DePhine from the upcoming Phobos sample return missions such as MMX (Fujimoto, M. 2017; Kuramoto et al., 2017). In addition, the mission will focus on the interior structures of both satellites.

2.1 Science Case 1: Interior Structure of Deimos and Phobos

The DePhine spacecraft will address the question of interior structure by various techniques, including gravity field mapping to high degree and order, direct radar observations to infer the structure of the upper layers of the moons, studies of rotational dynamics, magnetic sounding, and gamma-ray / neutron flux detections.

2.1.1 Mass and Gravity Field

The knowledge of the gravity field when combined with other bulk parameters, such as shape, volume, bulk density, porosity, and water ice content are key information for models of internal mass distribution, structure, composition, and Deimos/Phobos origins. Using data from X-band radio tracking during recent spacecraft flybys, especially by Mars Express (Andert et al., 2010; Pätzold et al., 2014b; Rosenblatt et al., 2008), the mass of Phobos has been estimated as $1.065 \pm 0.016\ 10^{16}$ kg (Pätzold et al., 2014a). The higher degree and order terms of the gravity fields (e.g., the C_{20} and the C_{22} terms) of Phobos suffer from large uncertainties (Pätzold et al., 2014b), due to the faint gravity signatures, the high spacecraft flyby speeds and the large flyby distances. Besides, even though the Phobos ephemeris has improved over the years (Lainey et al., 2007; Jacobson, 2010; Lainey et al., 2016), the Phobos positions relative to the spacecraft during the flybys were poorly known. For Deimos, only rough mass estimates from the early Viking flybys and from secular modeling are available, i.e., $1.51 \pm 0.04\ 10^{15}$ kg (Jacobson, 2010).

DePhine will move in "quasi satellite orbits" (see description later in the text), close to Deimos and Phobos, supported by optical navigation. Benefitting from a state-of-the art radio science experiment, even small spacecraft trajectory perturbations are revealed by the Doppler shift of the radio carrier. Effects of non-gravitational perturbations, e.g. solar radiation pressure and atmospheric drag as well as spacecraft control maneuvers (or wheel-off-loadings), will be carefully modeled in the process.

While the current knowledge of Phobos' mass has an uncertainty of about 18% (and higher order gravity parameters have uncertainties larger than the actual derived values) (Pätzold et al., 2014), the DePhine radio tracking will determine the mass at an accuracy of 0.01 %, the second degree and order gravity field coefficients at 1 % accuracy and the degree and order five gravity field coefficients at 50 % accuracy.

2.1.2 Shape and Rotation

Early attempts to derive Deimos and Phobos shape models were based on Mariner 9 and Viking TV camera images. These included tri-axial ellipsoids (Duxbury, 1974) or spherical harmonics representations. Duxbury (1991) determined over 300 control points, to solve for a Phobos shape model represented by of a spherical harmonics function with degree and order 8. Primarily based on limb as well as terminator observations Simonelli et al. (1993) and Thomas (1989) derived a 2° x 2° gridded shape model. The models have a relative accuracy ranging between +/-70 m and +/-50 m with locally larger uncertainties due to limited surface coverage. Willner et al.(2010; 2014) produced Phobos shape models using image data from the High Resolution Stereo Camera (HRSC) (Jaumann et al., 2007) and the Super Resolution Channel (Oberst et al., 2008) on-board the Mars Express spacecraft. A gridded Digital Terrain Model (DTM) (grid spacing: 100 m; relative accuracy: 25 m) and a spherical harmonic model (degree and order 45) were derived (Willner et al., 2014). With improved shape models, Phobos is estimated to have a volume of 5742 ± 35 km^3 (Willner et al., 2014). The volume of Deimos has been determined from Viking images as 1017 ± 130 km^3 (Thomas, 1993).

Both, Deimos and Phobos are in a locked rotation. Owing to their odd shapes and their slightly elliptic orbits, the satellites are undergoing physical librations. The librational amplitude of Phobos was

determined from direct observations and control point tracking by Mars Express and Viking Orbiters (Burmeister et al., 2014; Oberst et al., 2014; Willner et al., 2010) as well as from the effect on Phobos' orbital motion (Jacobson, 2010; Lainey et al., 2016). Reported libration amplitudes vary from 0.99° to 1.2° ± 0.15°, corresponding to a displacement at the equator of approximately 230 to 280 m. For Deimos, moving at larger distance from Mars in an orbit of smaller eccentricity, the amplitude of libration is predicted from the given orbit, gravitational interaction with Mars, and the shape model as 0.2° (20 m at the equator) (Rubincam et al.,1995), which remains to be verified.

DePhine will survey Deimos systematically and globally with a higher resolution than any other spacecraft before, which will result in higher-accuracy on both, shape and rotation parameters. For example, DePhine will allow to derive volume estimates for Deimos with uncertainties in the order of 1% and better (currently above 10%) and a first observation of the librational motion of Deimos will be possible. For Phobos, DePhine will collect high-resolution topographic data, especially during the very close and low-velocity flybys, which will refine our shape models and fill gaps in our current coverage.

2.1.3 Interior Models

Our current knowledge about the interiors of Deimos and Phobos is almost entirely based on indirect conclusions from estimates of mass, shape, and rotation. From the improved mass and the volume of Phobos and Deimos, the bulk densities of the two satellites have been estimated as 1.860 +/- 0.02 g/cm^3 (Willner et al., 2014) and 1.48 +/- 0.22 g/cm^3 (Rosenblatt, 2011) respectively, suggesting that their interiors have a high porosity and/or contain water ice (Avanesov et al., 1991; Murchie et al., 1991). The respective required porosity ranges are between 10-30% (Murchie et al., 1991) and 33-66 % (Rosenblatt, 2011), which are comparable with porosities of small-sized asteroids (Britt et al., 2002). This attests to an accretion process in which large blocks form an initial core with abundant voids that smaller debris are unable to fill andwould support origin scenarios from a planetary debris disk (Citron et al., 2015; Craddock, 2011; Rosenblatt and Charnoz, 2012; Rosenblatt et al., 2016). The low density can also be explained by sufficient water ice in the satellite interiors, depending on rocky material density and porosity. Detection of ice repositories would provide a strong constraint on the moons origins. However, neither the proportions of rock and water nor the origin of Deimos and Phobos can be constrained by the bulk density alone (Pätzold et al., 2014a; Rosenblatt, 2011).

Phobos' shape models together with models of rock-water ice mixtures have been used to predict moment of inertia coefficients of the satellite (Willner, 2009; Rosenblatt et al., 2009). These may be tested against observed Phobos libration amplitudes and gravity field coefficients, following dynamic theories (Borderies and Yoder, 1990). However, the observed shape models, libration amplitudes and the (poorly constrained) gravity parameter C_{20} can be brought in agreement with a wide variety of compositional models including a homogeneous mass distribution. Also, knowledge of obliquity, i.e., the tilt of the rotational axis with respect to the orbit plane is critical, which is currently assumed to be zero. The DePhine mission will improve our knowledge on the interior structure, mass distribution, shape, and volume by various techniques leading to improvements in uncertainty i.e. for the bulk density of Deimos by at least 10% to 1% or better.

2.1.4 Subsurface Structure

In order to discriminate among the various formation scenarios of the Martian satellites, sophisticated experiments directly observing the interior are needed that constrain the subsurface structure and bulk composition. Secondary radar echoes were revealed by MARSIS on Mars Express (Picardi et al., 2004) during Phobos flybys, but analyses of the data remained inconclusive. Shape models of Phobos were used to produce simulations of radar backscattering to separate surface from subsurface echoes (Plettemeier et al., 2009). Unfortunately, no echoes could be positively identified as coming from the subsurface. This can be attributed to the comparably large flyby distances to Phobos and the high relative velocities between spacecraft and target of 3 km/s limiting the performance of MARSIS by short effective integration times. The horizontal resolution of MARSIS in combination with the irregular shape of Phobos resulted in a Signal to Noise Ratio (SNR) of 25 dB in this best case, while a SNR of 50 dB has been achieved with MARSIS on a flat Mars surface under similar conditions. In addition, Phobos' fragmentation might be invisible to the MARSIS radar as fragment block sizes might be smaller than the applied wavelength (50-150 m). Furthermore, rocks with high metal content and carbonaceous chondrites are materials known with high dielectric loss properties resulting in possible signal absorption by Phobos' loose material.

The DePhine spacecraft will overcome the issues experienced with Mars Express flybys. The quasi synchronous orbit allows for longer integration times as the relative velocity will be in the order of less than 5 m/s. The radar package consists of a high frequency and low frequency channel optimised for the DePhine mission (see Section 4.1).

Magnetic field measurements can be used to support subsurface sounding and determine the conductivity or resistivity of the body's interior based on the induced response to the variable environment (Constable and Constable, 2004). The measurements indicate the intensities and spatial variability of remnant magnetic characteristics of the exposed surface as well as rocks down to several kilometers below the surface (Veselovsky 2004). The detection of a remnant magnetic signature on these moons would support the hypothesis of an impact-related formation scenario, during which magnetized crustal rocks (Acuña et al. 1999) were ejected from Mars as a consequence of the large impact event, and re-accreted in orbit (Citron et al. 2015; Ramsley & Head 2013a; Rosenblatt et al 2016). In contrast, the lack of a magnetic signature would give arguments in favour of the captured asteroids formation scenario. For example, magnetic investigations during the Rosetta mission document that primitive planetary rocks, such as the carbonate chondrite of 67P/Churyumov-Gerasimenko, do not have any significant remnant magnetism (Auster et al. 2015).

Measurements of the intensity and orientation of the remnant magnetic signatures will allow us a mapping of minerals with remnant magnetism for both moons. In concert with shallow surface radar and gravity data the magnetometer measurements will improve the knowledge on compositional variations of different types of rocks as well as ice and/or voids (e.g. Basilevsky et al. 2014, Pieters et al. 2014). This will support advanced models of the moons' structures and new scenarios for their origins.

2.1.5 Bulk Chemistry

The competing theories for the formation and early evolution of Mars' moons make distinct predictions for their present-day surface composition (e.g., Murchie et al., 2015), and measurements of elemental compositions can distinguish between competing hypotheses of Phobos' and Deimos' origin (Figure 1).

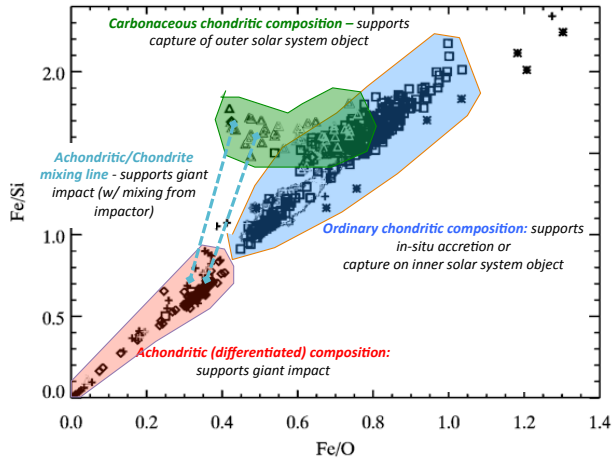

Figure 1: Measurements of Fe, Si, and O to distinguish between competing hypotheses of Phobos' and Deimos' origin (Figure adopted from Peplowski et al., 2015)

Gamma-ray and neutron spectrometer measurements can therefore test the existing formation models for Phobos and Deimos. For example, measurements of Fe, Si, and O concentrations can place Phobos and Deimos on the plot of Figure 1, which discriminates between the differentiation state of materials (i.e. achondrites vs chondrites), and by extension, separates out different formation scenarios. Measurements of additional elements (H, Mg, and K) as well as thermal, epithermal, and fast neutrons (Elphic et al., 2016) can provide the additional information needed to constrain the formation scenarios of Phobos and Deimos.

Gamma-ray and neutron spectroscopy represent established techniques for characterizing the elemental composition to tens of centimeters depth of planetary surfaces from orbit (see Section 4.4). Detected gamma-ray and neutron fluxes are converted to elemental concentrations using standard techniques (Lawrence et al., 2013; Peplowski et al., 2012). Note that DePhine currently does not foresee carrying a spectrometer, which would map the abundance of mineral compounds of very-near-surface regolith layers only.

2.2 Science Case 2: Deimos and Phobos Diversity

Perhaps the one most intriguing single observational fact in the question for the origin of the Martian satellites is that there exist two of them – not more and not less! Comparative studies of the two satellites will very much help understanding their formation. Are the two satellites siblings that have originated from the same source and by the same process? Or did they form separately through different events at different times?

The two satellites are generally similar but also strikingly different in some details. Both move in near-circular near equatorial orbits about Mars. However, Phobos is moving deep inside the Mars-synchronous orbit (subject to tidal decay and disruption), whereas Deimos is moving safely outside the synchronous orbit. The spectral characteristics of Phobos and Deimos – spectral slopes and absorption bands – are similar (Freaman et al., 2014). Also, both satellites show a low albedo (Pieters et al., 2014). However, the bulk densities differ substantially (Murchie et al. 2015). The visual appearance of the surface morphologies are quite different as well. Currently, meaningful comparisons between the two satellites are difficult, as the data volumes and knowledge is far more limited for Deimos. The comparative studies are aggravated as both satellites are affected differently by their environments. Phobos moves deep in the gravity field of Mars and is much affected by gravitational interaction in the satellite system. Mars ejecta is certainly deposited on Phobos and may or may not have formed the prominent groove structures (Murray and Heggie, 2014; Murray and Iliffe, 2011; Ramsley and Head, 2013a; b). Both, Phobos and Deimos are differently affected by the meteoroid bombardment from various solar system sources. Solar wind interacts with the surfaces in complex ways and is responsible for effects of space weathering.

2.2.1 Orbital Motions and Gravitational Interactions

The orbits of Phobos and Deimos are highly indicative for various dynamic parameters of the Martian satellite system. Because the static gravitational field of Mars is well constrained today, it is the gravity fields of the moons themselves, simultaneously with their physical libration, that will be accurately quantified from the satellites' secular orbital motion. DePhine data will tightly constrain the gravity fields of the bodies.

2.2.2 Meteoroid Flux from Crater Statistics and Dust Impact Detections

Small and large meteoroids from various solar system sources intercept the Martian satellite system, as attested by the large numbers of impact craters on Mars, Phobos, and Deimos. While the impact craters represent a powerful tool to study surface ages, craters can also be used to study the characteristics of the impactor population (Christou et al., 2014). As Phobos and Deimos are both locked in their orbits, impact rates and speeds vary across the surfaces of the satellites.

Christou et al., (2014) simulated the production of craters on Phobos from the sporadic flux of Mars-crossing asteroids and comets predicting a significant difference in the crater production rate on the leading and trailing hemisphere of Phobos. While the current crater statistics (limited by strong observational biases in the image data) do not support such a difference, accurate global crater counts by DePhine down to the smallest sizes will constrain this important effect. For unknown reasons, Deimos presents a lower number of large-sized impacts than Phobos (Thomas et al., 1992; Thomas et al., 1996).

Mars and its satellites should also intersect a number of meteoroid streams produced by comets. However, the predicted timing and geometry of the stream encounters (see Christou et al., (2014) and references therein) have not been observationally confirmed to-date. Such streams affect the Martian upper atmosphere in a measurable way (Grebowsky et al., 2002; Molina-Cuberos et al., 2003), as was

directly observed during the recent close encounter of comet C/Siding Spring with Mars. Our observations will constrain the flux of exogenous material to the Martian atmosphere and surface, including the delivery of organic compounds. DePhine will study the meteoroid encounters by using two complementary techniques: On one hand, we will study the crater population and size frequency distributions of craters on both satellites by imaging. We will search for hemispheric asymmetries in the distributions of the craters. On the other hand the dust detector in orbit will allow us to directly measure the mass distributions and motion vectors of smaller meteoroids.

2.2.3 Ejecta Production, Re-Accumulation, and Ring Formation

Large blocks and boulders of meter-scale cover the surface of Phobos, probably representing ejecta from impacts at the large end of the size scale, in particular from formation of crater Stickney. However, due to the observations from varying spacecraft ranges, only small areas on Phobos could be imaged at sufficient resolution for detection of blocks and boulders. In fact, almost all data have been obtained during a unique Phobos flyby of the Mars Reconnaissance Orbiter in 1998 (Thomas et al., 2000). DePhine, under suitable lighting conditions, will enable surface coverage for both moons with a globally uniform image resolution (<4 m/pixel; see Section 4.2). Thus, in contrast to previous missions, DePhine images will provide unbiased maps of block abundances, which will allow us to test hypotheses for the sources of blocks and the dynamics of their emplacements.

In addition to the above-mentioned bombardment by meteoroids (10^{-18} g < mass < 10^{2} g, velocity of about 15 km/s), the surfaces of Phobos and Deimos are exposed to solar ultraviolet radiation, solar wind plasma, and cosmic rays. The sputtering causes dust particles from the regolith to be ejected from the surface and to escape. With ejection- larger than escape velocity (about 10 m/s for Phobos and about 6 m/s for Deimos), but smaller than the orbital speed of the moons (V_{Ph}=2.1 km/s for Phobos and V_{D}=1.35 km/s for Deimos), particles should remain trapped in the Martian satellite system. Theoretical models (Banaszkiewicz and Ip, 1991; Ip and Banaszkiewicz, 1990; Ishimoto and Mukai, 1994; Juhász and Horányi, 1995; Kholshevnikov et al., 1993; Krivov and Hamilton, 1997) suggest that these dust grains form rings or tori along the orbits of the satellites.

Although the existence of such dust rings near Phobos/Deimos orbits has been predicted more than 40 years ago (Soter, 1971), no confirmed observations of rings or tori are available. Evidence for the presence of a dust or gas in the moons' orbits, related to a possible outgassing from their surfaces, may come from magnetic field observations. Fanale and Salvail (1989) did not find any evidence for outgassing from Phobos. With no detection of oxygen ions from a distance of 100 km, the upper limit for Phobos outgassing is set at < 10^{20} s^{-1}. A detection was reported by Dubinin et al., (1990; 1991) and Baumgärtel et al., (1998) using the Phobos-2 magnetometer data. On the contrary, Øieroset et al., (2010) found no direct evidences in the Mars Global Surveyor magnetometer data to support the idea of a significant outgassing or dust escape from the Phobos surface. More direct observations attempts by cameras also have remained inconclusive. The cameras on Viking 1 Orbiter and the Hubble Space Telescope (HST) lacked the required sensitivity (Krivov et al., 2006), while the Mars Express SRC (Super Resolution Channel) suffered from image blur and straylight (Oberst et al., 2008). DePhine is moving in favorable rendezvous orbits for new efforts to detect dust rings by its onboard camera. The spacecraft

data will deliver new models and bounds for volatiles near the surface and outgassing. Also, DePhine will study the population of micrometeoroids by means of a dust detector. Encounters with meteoroid streams will temporarily bolster the ejecta production rate from the surfaces of the moons. In turn, this will generate a proportionate enhancement on the density of the Phobos/Deimos dust tori (Zakharov et al., 2014) and lead to increased impact rates on the detector.

2.2.4 Ejecta from Mars

Phobos and Deimos, moving close to Mars, almost certainly have accumulated Mars ejecta in the past. Dynamic studies suggest that regolith may contain 0.0002 % to 0.025 of Mars material (Chappaz et al., 2012; Ramsley and Head, 2013a), with the thickness of deposited regolith layers varying from the near to the far side (Thomas et al., 2000). Hence, space explorers have identified Phobos and Deimos as targets, from where recovery of Martian samples may be comparably straightforward.

Investigators suggest that the various families of Phobos grooves may have formed as a result of such ejecta (Murray and Heggie, 2014). Alternatively, grooves may be surface manifestations of a global fracture pattern that pervades Phobos' interior (Asphaug and Melosh, 1993; Fujiwara and Asada, 1983). Recent theoretical work has reproduced similar formations on Vesta as the result of shear deformation following a large impact (Stickle et al., 2015; Scully et al., 2014). We will test this scenario by determining the internal structure of Phobos by radar. Like in the case of the craters, the current statistics of grooves suffer from observational biases. Also, with the current limited observational data, no grooves have been identified on Deimos. The camera will carefully map the surfaces of the two satellites to establish unbiased catalogs and maps of grooves. Using crater statistics, we may identify the sequence of groove formations and families of common origin. Spectral data and albedo patterns, which represent different mineral and physical properties of the regolith, will help in the mapping of the grooves (Longobardo et al., 2015). Studies of groove morphology will allow us to test their proposed origins.

Using radar mapping from orbit, we will assess regolith thickness for Phobos and Deimos, and variations of regolith thickness of near and farside. Using GRNS (Gamma Ray and Neutron Spectrometer) mapping from orbit, DePhine will be able to constrain the abundance of Mars material in the regolith, as GRNS may be able to discriminate between chemical compositions on the near- and farside, polar, and equatorial areas.

2.2.5 Regolith Formation

Studies of the Phobos' surface by OMEGA spectrometer on Mars Express (Fraeman et al., 2012; Gondet and Bibring, 2010) reveal that the surface is covered by a thick regolith layer, which appears rather uniform. In fact, the surface on Deimos appears smoother than the surface of Phobos, implying that morphologic features on Deimos have been gardened more effectively by impact ejecta and mass movements or that they simply never formed. The DePhine camera system will study the morphology of the Martian satellites to determine regolith characteristics, and to identify creep or mass wasting processes. Using the radar and GRNS experiments, DePhine will measure regolith thickness, its porosity, and elemental abundances. Multiple imaging at different phase angles will be used to study photometric

properties for interpretations of the physical properties of the surface regolith. The DePhine mission will provide the first opportunity to study the nature of space weathering effects on the Martian Moons. The HFC (High-Frequency Channel) radar will permit to study the relevant surface processes on these objects. The presence of large grains and blocks (cm to m) as well as peculiar regolith processes (migration, sorting) can be determined through the HFC observables (presence of layering, variation in the intensity of the radar echo, presence and distribution of radar scatters in the subsurface).

2.2.6 Tidal Interaction and Processes

The orbit of Phobos is known to decay due to tidal interaction with its parent planet Mars (Bills and Comstock, 2005; Burns, 1978). Hence, Phobos is experiencing increasing tidal forces, associated with accelerated rotation rate and centrifugal forces, which have been demonstrated to affect surface processes (Davis et al., 1981; Thomas, 1993). Studies of Mars Express high-resolution image data suggest that the evolution of Phobos' dynamic environment has triggered landslides on crater walls (Shi et al., 2016), perhaps as recently as within the past 10^8 years. The effects may be responsible for observed asymmetries for many of the Phobos' craters. Unfortunately, detailed studies of the surface of Phobos – not to mention Deimos – are hampered by the limited resolution and coverage of spacecraft images as well as the limited topographic data. DePhine will provide new and updated shape models for Deimos and Phobos, respectively, along with gravity field models, from which slopes (and evolution of dynamic slopes over time) may be determined. We will search for slopes near angle of repose and associated landslides. We will use high-resolution imaging to provide a complete global mapping of landslides associated with crater statistics to determine ages of such landslides and the associated time scales of processes.

2.2.7 Solar Wind Interaction

The surfaces of Deimos and Phobos are exposed to the solar wind. Multispectral observations reveal obvious effects of "space weathering" in areas where recent resurfacing is known to have exposed fresh material. Spacecraft spectral measurements for the surfaces of the satellites reveal two materials distinguished mainly by slope of the spectral continuum: a "redder" unit that dominates Deimos and is also present on Phobos, and a "bluer" unit excavated from depth on Phobos by the formation of Stickney crater (Murchie and Erard, 1996; Murchie et al., 1991; Rivkin et al., 2002; Thomas et al., 2011). Both Phobos' redder unit and Deimos indicate absorptions due to Fe-phyllosilicate near 0.65 μm (Murchie et al., 2008) and possibly olivine/pyroxene near 1 μm (Gendrin et al., 2005). Thermal infrared spectra show emission features consistent with phyllosilicates (Giuranna et al., 2011). Unfortunately, multispectral data for Phobos (not to mention Deimos) are limited in spatial resolution and do not show the needed details of fresh surface exposures on impact craters or mass wasting features. While DePhine does not carry a spectrometer system, the spacecraft onboard camera with its multiple color channels will be able to identify "red" and "blue" units and outline their extent at high spatial resolution. Thus, we may resolve local resurfacing events and improve our understanding of space weathering effects. By studying color variations in the context of geologic settings, it will be possible to understand whether observed color variations are related to exogenous or endogenous processes

As part of studying the diversity of Deimos and Phobos, DePhine will also more directly study the solar wind interactions. The two satellites are small non-conductive rocky bodies and normally expected to fully absorbing plasma impinging on them. However, recent Lunar missions, Chandrayaan-1 and Kaguya, discovered that the lunar regolith reflects only few % protons (Saito et al., 2008), but backscatters up to 20 % hydrogen (Wieser et al., 2009). A similar effect may be expected for the regolith surfaces of the Martian satellites. Indeed, backscattered protons were tentatively observed during a Phobos flyby of Mars Express from a distance of ~500 km, with a backscattered efficiency of 0.5-10 % (Futaana et al., 2010). Surprisingly, no such disturbance was observed during the closest-ever flyby on December 29, 2013, 07:09 UT at a distance of 58 km from the center of Phobos. This may be due to low solar wind speed and Phobos being likely inside the induced magnetosphere. Hence, the interaction of Phobos and Deimos with the environment and how plasma interacts with their regolith surfaces remains to be established.

Further clues on how plasma interacts with the regolith surfaces and on surface weathering processes may come from magnetic field investigations. Solar wind sputtering is a significant mechanism, which may alter surface properties (Murchie et al., 2014; Pieters et al., 2000) and release surface material to contaminate the surrounding environment as, e.g., in case of Mercury's polar regions (Paral et al., 2010). Also, a local field produced by magnetic anomalies could affect the surface properties as seen in the form of "swirls" on the Earth's Moon (Bhardwaj et al., 2015). However, the data coverage of currently available magnetic field observations for Phobos and Deimos is very limited and longer period observations from quasi-orbital motion are needed in order to see the relevant magnetic signatures. The magnetometer will also measure intensities and variation of external magnetic field of the satellites at different distances over the time of the mission. Such external magnetic signatures are generated by the interaction of the moons ionospheres with the solar wind (e.g. Baumgärtel et al. 1998; Øieroset et al. 2010, Poppe et al. 2015). The results of these measurements will contribute to the interpretations of the ionosphere composition derived from analyses of other instruments data and the dust analysis (Zakharov et al. 2014). DePhine will address the question of how the solar wind interacts with Phobos' regolith and how this might depend on solar activity or surface characteristics.

3 Mission Profile

3.1 Launch and Cruise

We anticipate a launch by ESA's future Ariane 6-2 vehicle, but unfortunately confirmed data about the Ariane 6-2 lift performance are not yet available for reliable mission planning at this stage. We adopt a Soyuz-Fregat launcher as the baseline, with which we can achieve a mission, which is technically feasible and which can accomplish all science goals well within the cost cap of the M5 program (550 Mio Euro). If Ariane 6-2 with improved performance becomes available, we propose an upgrade and modified mission profile (see further below).

The DePhine spacecraft will be launched into a Mars Transfer Orbit (MTO) with 1.5 revolutions about the sun. With the general time window given for the M5 mission opportunity (and with reasonable delta v),

this is the only viable transfer solution. Our baseline launch is on September 23, 2030, with hyperbolic excess velocity v_{inf} = 3.727 km/s and a Declination of the Launching Asymptote (DLA) of -1.8°. At this launch opportunity, the Soyuz launch vehicle will be able to inject a total S/C mass of ~1493 kg into MTO (including launch error margin). Several other opportunities for launch exist in 2030, days before and after the nominal launch date, which feature quite similar transfer time and spacecraft carrying capacity. No mission opportunity exists until two years after (2032), when a launch window opens again, which we consider as a backup. Here again, mission profile and spacecraft performance are similar to the nominal mission scenario.

While the Earth departure velocity will be provided by the launch vehicle, mid-course corrections and orbit insertion are performed through spacecraft thrusting maneuvers. For Mars capture with C3=0 km²/s² (parabolic orbit), a total velocity increment (Δv) of 670 m/s is required. We add a margin of 10% for "gravity loss" (accounting for non-zero duration of thrusting maneuvers) and other uncertainties. We choose an initial elliptical 300 km x 150,000 km orbit (height above ground) about Mars (similar to the arrival orbit of Mars Express) and perform a small inclination change to match Mars' equatorial plane, which requires an additional 81 m/s, to which we add a margin of 5%. This leads to a total Δv of 822 m/s, required for full orbit insertion. Mars orbit insertion is on January 30, 2033.

3.2 Science Mission Baseline

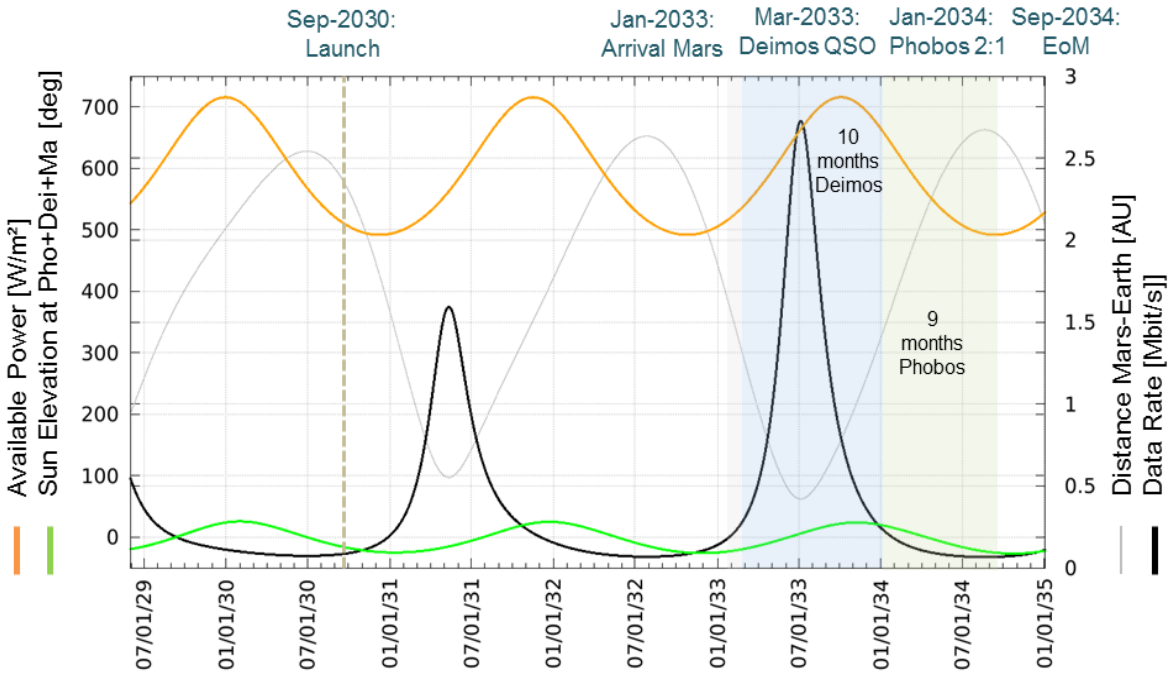

Figure 2: Mission timeline

In this initial high elliptical orbit, maneuvers are performed, which will adjust inclination, raise the periapsis and circularize the orbit of the spacecraft to enable a Deimos rendezvous and begin its science mission in March 2033. After 10 months of operations at Deimos, DePhine will change from its near-circular into an elliptic Mars orbit to carry out repeated encounters with Phobos for another 9 months. The mission will end in September 2034, just before Mars enters superior conjunction, when communication with Earth is disrupted. The total mission duration is 4 years (see Figure 2).

3.3 Deimos Quasi-Satellite Orbit

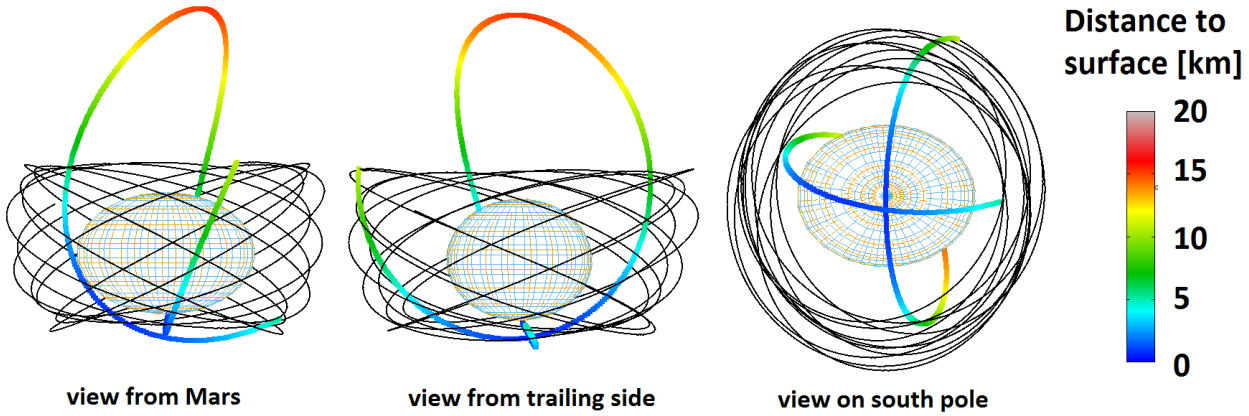

Figure 3: Quasi-Satellite Orbit and example of flyby maneuver (color-codes show distance to surface,)

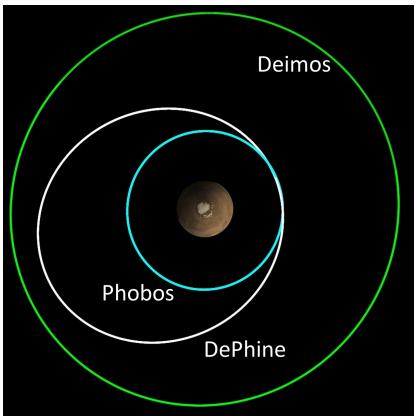

Figure 4: DePhine orbit (white) in 2:1 resonance with Phobos, with respect to the orbits of Deimos (green) and Phobos (blue)

Due to the low mass of the Martian satellites and the strong perturbation by Mars' gravity field, it is not possible to orbit the moons directly. Instead, DePhine will move in Quasi-Satellite Orbits (QSOs), which are in 1:1 resonance with the satellite orbits about Mars, but have slightly different inclinations and eccentricities. The orbital parameters of the Deimos QSOs are chosen such that the distance from the surface to DePhine will vary between 8 and 12 km, at relative speeds of 2-3 m/s and such that sub-spacecraft points move between 30° latitudes North and South ("quasi" inclination of 30°). Our numerical simulations, which were carried out using a variety of Deimos gravity field models, planetary perturbations, and radiation pressure effects, reveal that this orbit is stable over time scales of more than one year. Therefore, only minimal orbit correction maneuvers are needed during this phase. The spacecraft will gradually approach Deimos from the arrival orbit to finally enter the QSO. Approach distances to Deimos will be reduced, as the mission proceeds and gravity field knowledge of Deimos improves.

During the QSO mission phase, the spacecraft will carry out special flyby maneuvers of Deimos at selected orbital/solar phases, which enable approaches within 1-2 km at flyby speeds of 3-4 m/s. Each flyby requires a small thrusting maneuver with a typical Δv of 5-8 m/s. The flyby "event" lasts about 3-5 hours, after which the spacecraft returns to the stable QSO (see Figure 3). During the flybys, the radar, magnetometer, gamma-ray and neutron spectrometer as well as the camera will operate simultaneously, while the spacecraft will maintain the radio link with Earth for performing the radio-science experiment. This will require the spacecraft attitude guidance to maintain instrument pointing at Deimos, while maintaining Earth pointing of the steerable antenna. In the mission baseline we foresee ten flybys, requiring 86 m/s of Δv.

The simultaneous radio tracking and image data acquisition allow us to make precise reconstructions of the flyby trajectories with respect to the targets. Otherwise, as in the case of Mars Express, currently the only spacecraft to carry out Phobos flybys on a regular basis, the flyby trajectory must be reconstructed from the tracking data before and after the flyby in combination with target ephemeris knowledge, a procedure sensitive to systematic errors.

3.4 Phobos Phase

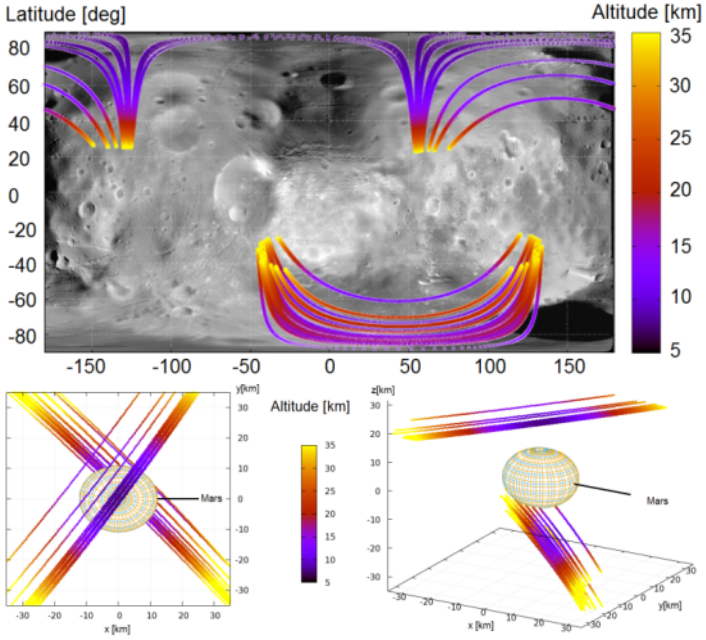

Figure 5: Polar flybys at Phobos. Spacecraft ground tracks in the body-fixed (top) and inertial reference frame (bottom).

After the Deimos phase, DePhine will perform thrusting maneuvers, to move from the near-Deimos circular orbit to an eccentric orbit, chosen to be in 2:1 resonance with the orbit of Phobos (pericenter of 9,238 km and an apocenter of 20,510 km) (Figure 4). We foresee approximately 45 Phobos flybys within a mission phase of 1 month (1.5 flybys per day) at moderate speeds of approximately 450 m/s (considerably less than the typical Mars Express Phobos flybys at speeds of approximately 3 km/s).

At the beginning of this mission phase, we will begin with safe flyby distances to Phobos of ~500 km. Benefitting from the flyby tracking experience and improving Phobos ephemeris data that will be obtained, we will then reduce the distance until DePhine achieves flybys below 50 km with respect to the center of Phobos. Small thrusting maneuvers near apocenter will allow us to change the flyby geometry, i.e., the intersection of the spacecraft trajectory with the so-called b-plane (the plane attached to the target, perpendicular to the spacecraft trajectory), which will allow us to carry out flybys over polar areas (typically more difficult to achieve from the QSOs). The closest approach will occur either slightly before or after S/C pericenter passage allowing us to realize different approach geometries (Figure 5). Remaining propellant permitting, flyby distances of 10 km, implying a small risk of collision, may be achieved at the end of the mission.

4 Onboard Instruments

The DePhine spacecraft shall carry seven instruments: a Shallow Subsurface Radar (SSR), a Wide Angle Survey Camera (WASC), a Deimos Magnetometer (DeMag), a Gama Ray and Neutron Spectrometer

(GRNS), the Gravity Radio Science Investigation of the Martian Moons (GRIMM), theeXtra Small Analyzer of Neutrals – 2 (XSAN-2) and the Dust In the Martian EnviRonment (DIMER).

4.1 Shallow Subsurface Radar – SSR

The SSR transmits radar waves to the surface of the Martians moons and will analyze the reflected and refracted sounding waves, to obtain information about the surface and internal structure of Deimos and Phobos. The radar is a dual channel radar consisting of a High-Frequency Channel (HFC) covering a frequency range from 300 - 3000 MHz and a Low-Frequency Channel (LFC) operating at 60 MHz with 20 MHz bandwidths. The design is optimized for DePhine's operation with altitudes ranging from 30 to 1 km and low orbital speed.

The High Frequency Channel will provide 2D radar images processing echoes from the surface and the first tenth of meters of the regolith in nominal mode. It will be able to detect layers, embedded rocks or possible water ice with depth depending decametric vertical resolution. By multiple coverage we will achieve the vertical resolution needed to image embedded structures: for DePhine, we foresee 3D tomography with metric resolution, which will require approximately 40 observation passes and acquisition sequences with different observation geometries. The reduction and correct 3D interpretation of the data will benefit from the high-resolution (a few meters or less) Digital Terrain Models (DTMs) of Deimos, delivered by the DePhine camera and associated photogrammetric image processing. Altimeter modes at higher frequencies are implemented to provide target ranges for both science and real-time navigation with a resolution of up to 6 cm. This information will contribute to shape model, surface roughness estimation, S/C orbit restitution, as well as to studies of Deimos' and Phobos' dynamical state.

The Low Frequency Channel will enable probing of the first few hundred meters of Deimos and Phobos and will allow us to assess whether the observed geological structures have vertical extensions. LFC will be able to detect hidden blocks, boulders or voids, which would hint at a rubble pile interior, critical information for possible formation scenarios.

The SSR consists of an electronic unit and an antenna system facing the surface. The electronic unit delivers a set of adjustable frequencies from 300 MHz to 800 MHz in HFC nominal mode and up to 3 GHz in the extended band. The fully polarimetric antenna system transmits a circular polarized signal and receives the returned signal in two perpendicular linear polarizations. Both signals are amplified, sampled, phase-calibrated and combined to co- and cross polarized signals in the two-channel receiver chain on board. The LF Channel is based on the bistatic Low-Frequency Radar (LFR), under development for the Asteroid Impact Mission (AIM) by ESA. It is a BPSK-coded radar operated at 60 MHz with a 10 to 20 MHz bandwidth corresponding to the monostatic mode of LFR on the AIM orbiter. The antennas will be accommodated on the S/C instrument deck. The typical half-power beam width of more than 90° is limiting the pointing requirement to about +/- 10° or less.

4.2 Wide Angle Survey Camera – WASC

The Wide Angle Survey Camera (WASC) instrument uses a frame sensor array in combination with a wide angle lens for Deimos and Phobos imaging. The main science goal is the mapping of geological structure

and diversity. The instrument will have a multispectral capability (including near-infrared) for compositional information. The camera will also carry out astrometric observations and will contribute significantly to spacecraft optical navigation, in particular on flyby sequences.

WASC will regularly take stereo sequences, which will be realized by overlapping nadir-pointed images, taken in close temporal succession, along the ground track of the spacecraft. While we benefit from the large field of view of WASC (25°), this allows us a significantly reduced operational effort. Image blocks will provide stereo information of equally high quality both along and perpendicular to the flight direction. In combination with the high geometric stability of frame detectors, 3D point reconstruction from stereo analysis will be accurate to scales significantly smaller than the image resolution.

The instrument is derived and re-uses main components from the NASA Dawn mission's framing cameras (Dawn FC) (Sierks et al., 2011) (see sample image and camera laboratory model, Figure 6, Figure 7), which in turn is based on the design of the European Space Agency's Rosetta Landing Imaging System (ROLIS) (Mottola et al., 2007). A major modification for WASC is its increased field of view (larger by a factor of about 5 compared to Dawn FC).

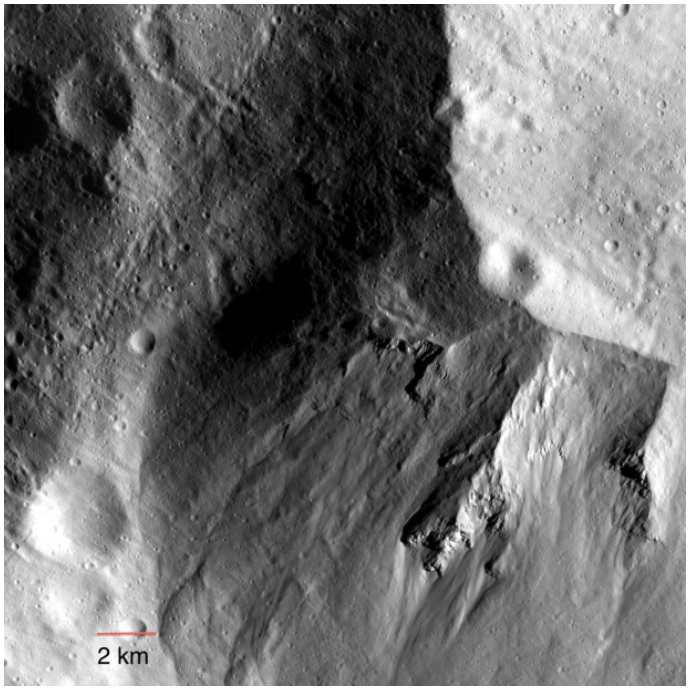

Figure 6: Rim of Matronalia Rupes on Vesta, example image from the Dawn framing camera (Fig. 7) Source: Planetary Data System F1b_FC21A0015600_11361133030F1A.

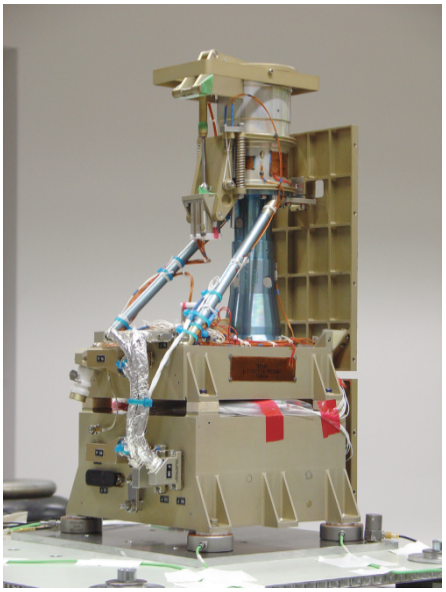

Figure 7: Dawn framing camera

WASC will be equipped with a refractive optics modified from the ROLIS camera of Rosetta (Mottola et al., 2007). The optics will be color-corrected and make use of radiation-tolerant glasses. With an effective focal length of 30 mm, it will project a square field of view (FOV) of 25° by 25° onto the Charge Coupling Device (CCD) detector. This translates to an image scale of 0.21 mrad per pixel. Image ground pixel size will be better than 4 m/pixel, on average, for global mapping (from 10 km distance), and as high as 90 cm/pixel on close flybys (2 km for close flybys of Deimos), gives a sampling of about 85 cm/pixel.

The detector in WASC is a 1k x 1k CCD with frame-transfer architecture, which allows the implementation of electronic shuttering, avoiding a mechanical solution. Color imaging will be realized by a filter wheel, which comprises an 8-position Geneva drive, a stepping motor, a Hall-effect angle encoder, and a wheel with 8 positions (specific filters yet to be determined). WASC exploits a compact architectural design coupled with a framing detector, avoiding any scanning mechanism or operational requirement on the S/C to obtain images in different spectral bands and in stereo.

4.3 Deimos Magnetometer – DeMag

DeMag represents a suite of magnetometry instruments. The main component is a three-axial vector compensated fluxgate magnetometer with a Mascot design (Hercík et al. 2016; Fig. 8). The principle of fluxgate magnetometers is based on measuring the induced field of a soft magnetic core which is excited by a periodic saturating magnetic field. Like a transformer the core is surrounded by a primary and a secondary coil. The primary coil is used to excite the core, and a secondary one measures the response. A third set of coils is providing a negative feedback to keep the sensor in linear regime. The information about the ambient magnetic field is acquired from the combination of the response and the feedback signals. The technological details of the secondary magnetometers have to be defined.

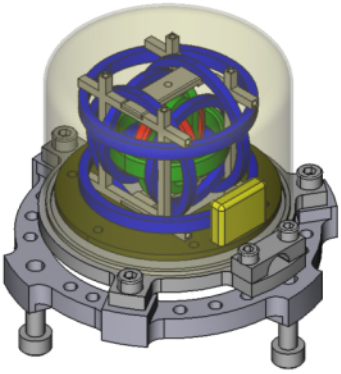

Figure 8: Fluxgate sensor MASCOT design (Hercík et al. 2016)

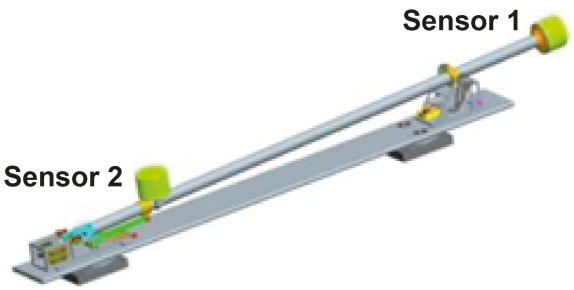

Figure 9: DeMag boom

We foresee that two magnetic sensors are mounted on a deployable short (1 m) boom at the outer edges of the S/C structure for keeping interference level low and for enabling separation of s/c interferences by a dual sensor method (see Figure 9).

4.4 Gamma Ray and Neutron Spectrometer – GRNS

Planetary gamma-rays and neutrons are created within near-surface material when galactic cosmic rays (GCR) collide with an airless or nearly airless planetary body. The GCRs liberate neutrons from elemental nuclei, which then generate gamma-rays via nuclear excitation reactions that are detected by sensors on orbiting (or landed) spacecraft. Bulk concentrations of a number of elements (e.g., Fe, Si, O, Mg, H) can be measured using these GCR-induced gamma-rays. In addition, the bulk concentration of some elements (e.g., K, Th, and U) can be measured using direct gamma-rays from their radioactive decay. Finally, GCR-induced planetary neutrons provide independent and complementary composition information through the three different energy ranges of thermal, epithermal, and fast neutrons. Thermal neutrons provide a measure of neutron absorbing elements (e.g., Fe and Ti), epithermal

neutrons enable a determination of hydrogen concentrations and fast neutrons provide analysis of average atomic mass.

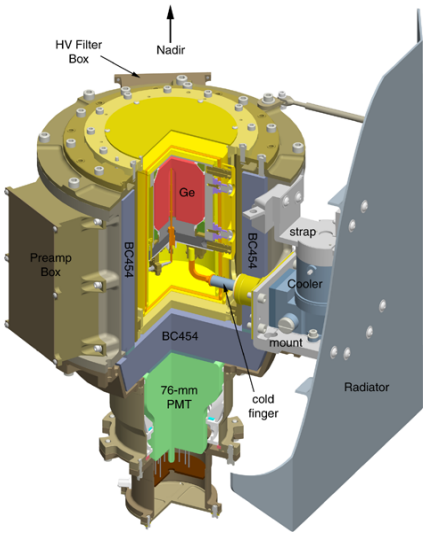

Figure 10: CAD model cutaway view of the GRS sensor (from Goldsten et al., 2007). The Germanium (Ge) crystal (5 cm in diameter and 5 cm in length) is highlighted in red. The intended view direction of the measurement is upward along the Ge detector centerline (same as the cut axis).

The goals of the Gamma-Ray and Neutron Spectrometer (GRNS) are to measure the elemental concentrations of Fe, Si, O, Mg, K, H, as well as thermal, epithermal and fast neutrons. The elemental concentrations are obtained with a relative statistical uncertainty of better than 20 %. The neutron measurements enable the compositional characterization needed to distinguish between the various Phobos/Deimos formation scenarios.

In order to make these measurements, GRNS needs to acquire data from Phobos and Deimos from a distance of less than one body radii for at least 20 hours per body. For the neutron measurements, the data can be acquired using standard neutron sensors that have spaceflight heritage from the Lunar Prospector, Mars Odyssey, Dawn, and MESSENGER missions.

The GRNS consists of four primary subsystems, namely a Gamma-Ray Spectrometer (GRS), a Neutron Spectrometer (NS), and two associated Data Processing Units (DPUs). The GRS is based largely on the MESSENGER GRS (Figure 10) (Goldsten et al., 2007), which is a High-Purity Ge HPGe gamma-ray sensor, which warrants precision measurements with a high signal-to-background ratio. The NS is based on the Lunar Prospector NS (Feldman et al., 2004) equipped with two ^{3}He gas proportional counters that are used to measure thermal and epithermal neutrons.

4.5 Gravity Radio Science Investigation of the Martian Moons – GRIMM

The radio science experiment uses the radio link between the spacecraft and the ground station antennas on Earth for a precise mass and gravity field determination. The experiment shall be supported by optical navigation.

The attracting forces of the small moons and other non-gravitational forces act on the spacecraft and change its trajectory and speed, which can be precisely extracted from the Doppler shift of the radio carrier frequency received on ground (for details see: Andert et al., 2010; 2015; Pätzold et al., 2011; Pätzold et al., 2014a; 2014b;). The mass and gravity field of the body when combined with the body´s volume and shape determined from camera observation, pose constraints on the bulk density and hint at the internal structure and composition and porosity considerations, as demonstrated during the Mars Express flybys of Phobos (Andert et al., 2010; Pätzold et al., 2014a; 2014b) and the Rosetta flyby at asteroid 21 Lutetia (Pätzold et al., 2011).

The Radio Science experiment GRIMM relies upon the on-board radio subsystem, which includes two redundant transponders providing a coherent two-way X-band uplink/X-band downlink (X/X) radio link, two redundant Travelling Wave Tube Amplifier (TWTA), which amplify the X-band downlink radio signal generated by the transponder, and the High Gain Antenna (HGA), which receives and transmits the radio signal. A hydrogen maser in the ground station is used as the frequency standard for generation/acquisition of the uplink/downlink signal.

The HGA shall be pointed towards the Earth during GRIMM gravity operations. The orbiter will not perform AOCS (Attitude and Orbit Control System) operations during GRIMM operation.

4.6 eXtra Small Analyzer of Neutrals - 2 – XSAN-2

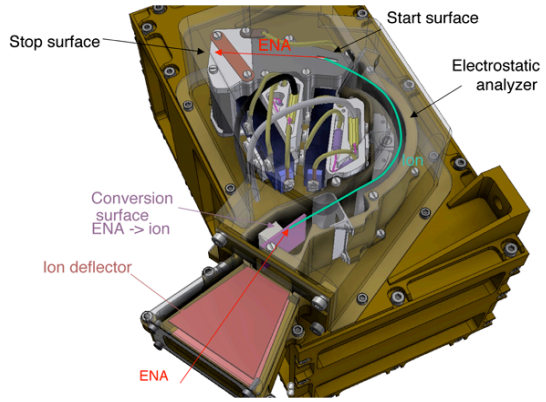

Figure 11: Cross section of the Analyzer of Neutrals (XSAN-2) and a sample trajectory of an Energetic Neutral Atom (ENA) to be detected.

The eXtra Small Analyzer of Neutrals – 2 (XSAN-2) is a compact sensor for measuring neutrals (with energy >10 eV; energetic neutral atoms, or ENAs) or ions released from the regolith. An entrance deflector can be switched on or off for rejection or detection of ions. Neutrals (and ions for deflector off) passing the deflector hit the conversion surface and are transformed to positive ions. These are guided to an electrostatic analyzer (ESA), which provides the energy determination. The ions enter a time-of-

flight section (TOF), which provides a rough mass identification within the accuracy determined by the energy conversion. The instrument sensor will be equipped with a cover to protect the instrument's sensitive surfaces from contaminations during AIV (Assembly, Integration and Verification) and launch. The cover is opened when safe operations become possible.

XSAN-2 (Figure 11) is a slightly modified replica in a series (Figure 12) of small ion and neutrals spectrometers built for Chandrayaan-1 (2008), Phobos-Grunt (2011), and it is going to fly on the BepiColombo mission (2018). More detailed description is found in Wieser and Barabash (2016).

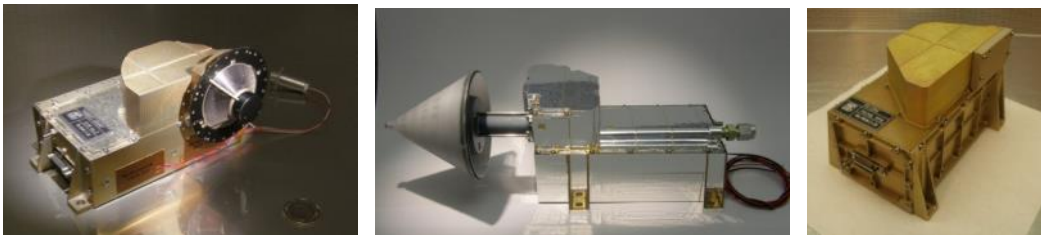

Figure 12: Selected flight models of the XSAN-2 series, from left to right: Phobos-Grunt/DIM, BepiColombo/MIPA, PRISMA/PRIMA (Wieser and Barabash, 2016).

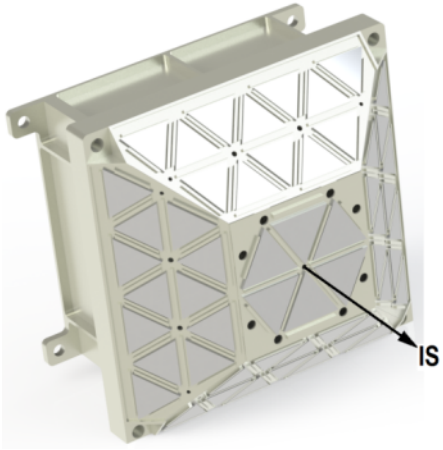

Figure 13: Impact sensor block

4.7 Dust In the Martian EnviRonment – DIMER

The DIMER experiment is devoted to detecting dust particles in the Mars environment, which have been suggested to form dust tori associated with the orbits of the Martian moons. Besides, the experiment will address the question of the presence of electrostatic fields causing levitating and escaping of dust particles from the Martian moons. The instrument includes two identical blocks of impact sensors (IS1 and IS2) and 12 small sensors (10 g each) based on piezoceramic compounds mounted on the solar panel for registration of dust particles hitting the spacecraft (see Figure 13). DIMER will be able to measure impact impulse, mass, velocity, and charge of the impacting particles. The instrument is inherited from

the Russian Lunar Dust Monitor (PmL), which will be a payload element on the Russian lunar landers scheduled for launch in 2019 and 2021. The PmL has passed all qualification tests (thermal, mechanical, electrical, functional, operation life time testing) and is now being manufactured. DIMER will use the sensor, electronics and mechanics developed for PmL

5 Space Segment

The scientific objectives of the DePhine mission can be fulfilled with a moderately complex space segment. The design has been confirmed with an internal phase 0 study, using the concurrent engineering design facilities at OHB System AG in Bremen, Germany. Subsystem trade-offs were considered and conservative assumptions were applied throughout the spacecraft design. At the time of writing, the performance of the Ariane 6 launcher is unknown. The mission has therefore been designed to be compliant with the known Soyuz launcher performance (i.e. uplift capability) from ESA's launch site in Kourou. The environmental loads, fairing dimensions, launch adapter and launcher-spacecraft interfaces were taken from the draft issues of the Ariane 6.2 user manual (ArianeSpace, 2016). Heritage is taken from previous NASA and ESA missions (Mars Global Surveyor, Mars Express, Rosetta, BepiColombo), and well-characterized concepts under study (Phobos Sample Return, MMX, AIM).

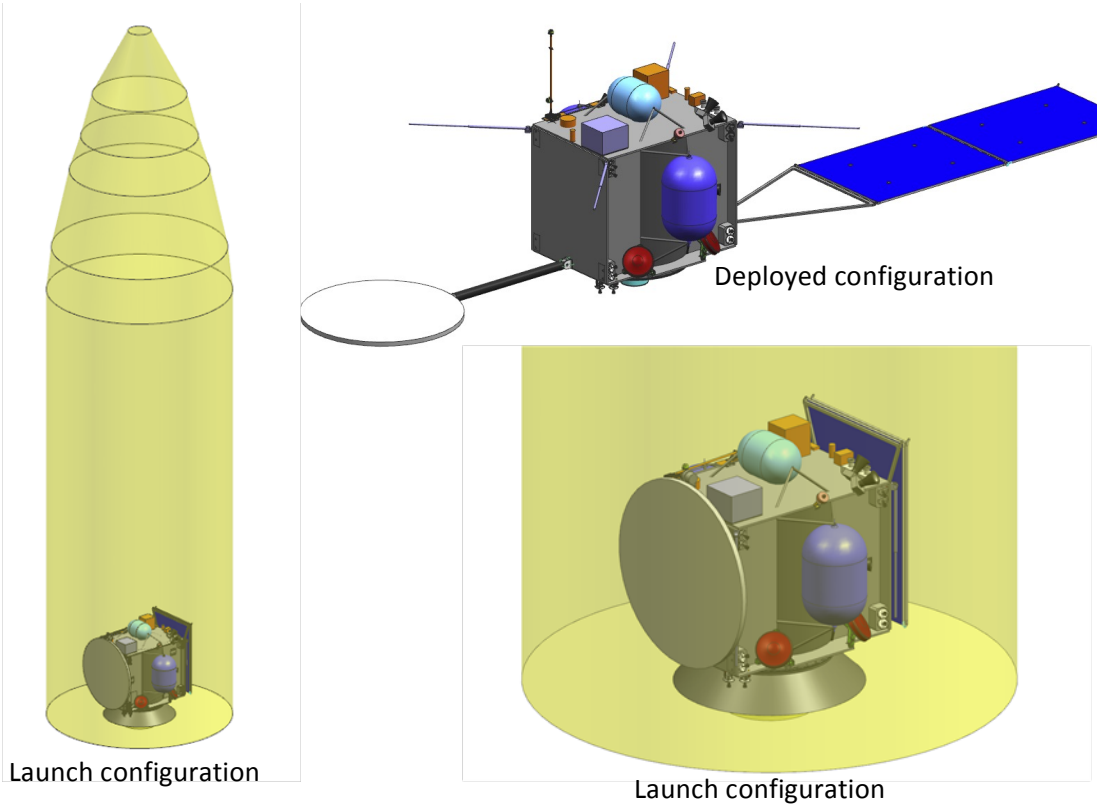

Figure 14: Spacecraft in launch and deployed configuration [OHB]. Note the steerable HGA and solar array panels.

Figure 14 shows the spacecraft in its deployed and launch configuration, respectively. The spacecraft has a total dry and wet mass of about 585 kg and 1210 kg at launch, including all margins. The payload contribution is about 40 kg. The delta-v demand requires about 545 kg of propellant. The launch adapter mass is 80 kg. A launch mass margin of about 12 % (or more than 160 kg) as compared to the Soyuz performance makes the design robust towards any potential mass growth and towards uncertainties of the Ariane 6 class launcher.

The top deck of the spacecraft is the dedicated payload panel, which points towards the nadir direction with respect to Deimos and Phobos. The solar array and HGA are accommodated on opposite sides of the spacecraft. This maintains the center of mass and limits the (low) disturbance torques in the Mars environment. The solar array can be rotated for Sun tracking (1 degree of freedom). The HGA is equipped with a two axis pointing mechanism to enable independent Earth-pointing capabilities. Mounting the HGA on a boom increases the pointing envelope and flexibility. Two propellant tanks, the helium tank and reactions wheels are mounted externally. Each are clad with micro-meteorite protecting Multilayer Insulation (MLI).

The spacecraft's structure is based around a central tube, which establishes the primary load bearing path. Additional shear webs and panels create compartments for internal accommodations and external mounting. The propulsion subsystem uses a common approach with a mixed oxides of nitrogen (MON)/ Monomethylhydrazine (MMH) bipropellant chemical system. Large orbit maneuvers are performed with an apogee engine located at the bottom of the central tube. Two sets of small thrusters are used for attitude control and to perform small orbit maneuvers. Propellant is accommodated in three different tanks. A single MON tank is located in the central tube with two smaller MMH tanks mounted to its sides. Helium is stored in a smaller pressurized tank. The driving demand for the power subsystem occurs when the spacecraft is in its flyby mode. The payload and communication system (for the radio-science experiment) are operated simultaneous for several hours. The deployable solar array is mounted on a single wing, similar to Mars Global Surveyor. It provides sufficient power at a reduced mass. The battery is sized for launch and early operations, and the worst-case eclipse duration caused by Deimos in QSO.

The Guidance, Navigation and Control (GNC) subsystem includes a standard suit of star trackers, Sun sensors, reaction wheels, an Inertial Measurement Unit (IMU) and a navigation camera. The GNC strategy is based on ground-in-the-loop guidance and navigation, with minimal on-board GNC autonomy. Delta-differential one-way ranging and offline landmark matching occurs before the spacecraft performs its injection maneuver into its flyby trajectory. Heritage is taken from previous missions (Mars Express, Rosetta) and possible future missions (Phobos Sample Return, AIM, PILOT project). The communication subsystem is based on an X-band system, with a steerable HGA. This steerable antenna will allow simultaneous radio tracking and observations by the platform instruments, which is technically not possible for the current Mars Express, with its antenna hard-mounted on the spacecraft bus.

Data downlink, varying with Mars distance (Fig. 2), is realized via the 35m antennas of ESA's ESTRACK. The data-handling subsystem implements a standard solution using an on-board computer, remote-terminal units and a solid-state mass-memory unit. The mass memory is capable of covering four days of

science and house-keeping data. A simple passive thermal control subsystem is used with a heater in a closed loop system.

While the mission baseline described above was analyzed in much detail, the feasibility of alternative mission concepts was also assessed. The different alternative mission configurations are summarized in Table 1.

Mass could be saved, for example, if the number of flyby events were reduced, or if the spacecraft entered a longer-period 3:1 Phobos resonance. The spacecraft could also first be injected into a GTO before its interplanetary transfer. Here, DePhine could be launched atop of Lisa-Pathfinder-derived propulsion stage (a jettison-able bi-propellant propulsion module) into GTO. This modified design, however, must be traded-off against increasing costs and complexity of the mission. This would avoid the redesign of the baseline structure and propulsion system to accommodate the increased delta-v. A dual-launch scenario on a co-manifested launcher might also be feasible.

Table 1: Overview of Alternative Scenarios.

Launcher	Scenario	Launch mass, kg	Margin, kg	Margin, %
Soyuz-FG	Baseline	1129	162	12%
	3:1 resonance	1119	172	13%
	Only 5 Deimos flybys	1113	178	13%
	ELECTRA UHF addition	1151	140	10%
Ariane 6-2	DePhine-A	1450	TBD	TBD Soyuz+12%
	GTO	1713	3287	66%
	GTO with propulsion stage	2531	2469	49%

Benefitting from the increased launcher performance of the Ariane 6.2, the nominal mission baseline can be upgraded (“DePhine-A”), resulting in a greater science return. For example, the spacecraft may go into a Phobos QSO after the resonant elliptical orbit. Entering the QSO requires the spacecraft to adjust its orbital parameters to match those of Phobos, at a significant cost of delta-v. In addition, an upgrade would allow the deployment of a small lander on Deimos. However, the added lander including deployment mechanisms and navigation capability, will add considerably to the launch mass of the spacecraft (Table 1). In fact, in these configurations, the total launch mass increases by 16 % w.r.t the baseline, and exceeds the Soyuz capability by 5 %. The option would become feasible if the performance of the Ariane 6.2 increased moderately.

Acknowledgements

The mission and system design for DePhine was developed by a consortium composed of teams from German Aerospace Center (DLR) and OHB System AG, as well as of scientists from international institutes and organizations. The authors acknowledge the subsystem support of OHB’s concurrent engineering facillity.

6 References

Acuña, M.H., Connerney, J.E.P., F. , N., Ness, Lin, R.P., Mitchell, D., Carlson, C.W., McFadden, J., Anderson, K.A., Rème, H., Mazelle, C., Vignes, D., Wasilewski, P., Cloutier, P., 1999. Global Distribution of Crustal Magnetization Discovered by the Mars Global Surveyor MAG/ER Experiment. *Science* 284, 790-793. doi: 10.1126/science.284.5415.790

Andert, T.P., Remus, S., Simpson, R.A., Pätzold, M., Asmar, S.W., Kahan, D.S., Bird, M.K., Häusler, B., Tellmann, S., 2015. First Rosetta Radio Science Bistatic Radar Observations of 67P/Churyumov-Gerasimenko, EGU General Assembly Conference Abstracts.

Andert, T.P., Rosenblatt, P., Pätzold, M., Häusler, B., Dehant, V., Tyler, G.L., Marty, J.C., 2010. Precise mass determination and the nature of Phobos. *Geophysical Research Letters* 37. doi: 10.1029/2009GL041829

ArianeSpace, 2016. Ariane 6 User Manual, Issue 0, Revision 1

Asphaug, E., Melosh, H.J., 1993. The Stickney impact of PHOBOS - A dynamical model. Icarus 101, 144-164. doi: 10.1006/icar.1993.1012

Auster, H.-U., Apathy, I., Berghofer, G., Fornacon, K.-H., Remizov, A., Carr, C., Güttler, C., Haerendel, G., Heinisch, P., Hercik, D., Hilchenbach, M., Kührt, E., Magnes, W., Motschmann, U., Richter, I., Russell, C.T., Przyklenk, A., Schwingenschuh, K., Sierks, H., Glassmeier, K.-H., 2015. The nonmagnetic nucleus of comet 67P/Churyumov-Gerasimenko. Science 349. doi: 10.1126/science.aaa5102

Avanesov, G., Zhukov, B., Ziman, Y., Kostenko, V., Kuzmin, A., Murav'ev, V., Fedotov, V., Bonev, B., Mishev, D., Petkov, D., Krumov, A., Simeonov, S., Boycheva, V., Uzunov, Y., Weide, G.-G., Halmann, D., Pössel, W., Head, J., Murchie, S., Schkuratov, Y.G., Berghänel, R., Danz, M., Mangoldt, T., Pihan, U., Weidlich, U., Lumme, K., Muinonen, K., Peltoniemi, J., Duxbury, T., Murray, B., Herkenhoff, K., Fanale, F., Irvine, W., Smith, B., 1991. Results of TV imaging of phobos - experiment VSK-FREGAT. *Planetary and Space Science* 39, 281-295. doi: 10.1016/0032-0633(91)90150-9

Banaszkiewicz, M., Ip, W.-H., 1991. A statistical study of impact ejecta distribution around Phobos and Deimos. *Icarus* 90, 237-253. doi: 10.1016/0019-1035(91)90104-2

Basilevsky, A.T., Lorenz, C.A., Shingareva, T.V., Head, J.W., Ramsley, K.R., Zubarev, A.E., 2014. The surface geology and geomorphology of Phobos. Planetary and Space Science 102, 95-118. doi: 10.1016/j.pss.2014.04.013

Baumgärtel, K., Sauer, K., Dubinin, E., Tarrasov, V., Dougherty, M., 1998. “Phobos events”—Signatures of solar wind interaction with a gas torus? *Earth, Planets and Space* 50, 453-462. doi: 10.1186/bf03352133

Bhardwaj, A., Dhanya, M.B., Alok, A., Barabash, S., Wieser, M., Futaana, Y., Wurz, P., Vorburger, A., Holmström, M., Lue, C., Harada, Y., Asamura, K., 2015. A new view on the solar wind interaction with the Moon. *Geoscience Letters* 2, 1-15. doi: 10.1186/s40562-015-0027-y

Bills, B.G., Comstock, R.L., 2005. Spatial and temporal patterns of solar eclipses by Phobos on Mars. *Journal of Geophysical Research* 110, E04004. doi: 10.1029/2003JE002209

Borderies, N., Yoder, C.F., 1990. Phobos Gravity-Field and Its Influence on Its Orbit and Physical Librations. *Astronomy & Astrophysics* 233, 235-251.

Britt, D., Yeomans, D., Housen, K., Consolmagno, G., 2002. Asteroid density, porosity, and structure, Asteroids III. The University of Arizona press, pp. 485-500.

Burmeister, S., Willner, K., Oberst, J., 2014. Phobos' Rotational Elements From Control Point Network Analysis: A New Analytic Approach, Vol. 9, EPSC2014-326-3, p. 326.

Burns, J.A., 1978. The dynamical evolution and origin of the Martian moons. *Vistas in Astronomy* 22, 193-208. doi: 10.1016/0083-6656(78)90015-6

Burns, J.A., 1992. Contradictory clues as to the origin of the Martian moons. Mars, pp. 1283-1301.
Chappaz, L., Melosh, H.J., Vaquero, M., Howell, K.C., 2012. Transfer of impact ejecta fragments material from the surface of Mars to Phobos and Deimos, AAS/AIAA Space Flight Mechanics Meeting, pp. 1-20.
Christou, A.A., Oberst, J., Lupovka, V., Dmitriev, V., Gritsevich, M., 2014. The meteoroid environment and impacts on Phobos. *Planetary and Space Science* 102, 164-170. doi: 10.1016/j.pss.2013.07.012
Citron, R.I., Genda, H., Ida, S., 2015. Formation of Phobos and Deimos via a giant impact. *ICARUS* 252, 334-338. doi: 10.1016/j.icarus.2015.02.011
Constable, C.G., Constable, S.C., 2004. Satellite magnetic field measurements: applications in studying the deep Earth, in: Sparks, R.S.J., Hawkesworth, C.T. (Eds.), The State of the Planet: Frontiers and Challenges in Geophysics. Washington DC: American Geophysical Association, Geophysical Monograph 150, pp. 147-159.
Craddock, R.A., 2011. Are Phobos and Deimos the result of a giant impact? *Icarus* 211, 1150-1161. doi: 10.1016/j.icarus.2010.10.023
Davis, D.R., Housen, K.R., Greenberg, R., 1981. The unusual dynamical environment of Phobos and Deimos. *Icarus* 47, 220-233. doi: 10.1016/0019-1035(81)90168-8
Dubinin, E.M., Lundin, R., Pissarenko, N.F., Barabash, S.V., Zakharov, A.V., Koskinen, H., Schwingenshuh, K., Yeroshenko, Y.G., 1990. Indirect evidences for a gas/dust torus along the Phobos orbit. *Geophysical Research Letters* 17, 861-864. doi: 10.1029/GL017i006p00861
Dubinin, E.M., Pissarenko, N., Barabash, S.V., Zacharov, A.V., Lundin, R., Koskinen, H., Schwingenschuh, K., Yeroshenko, Y.G., 1991. Tails of Phobos and Deimos in the solar wind and in the Martian magnetosphere. *Planetary and Space Science* 39, 123-130. doi: 10.1016/0032-0633(91)90134-V
Duxbury, T.C., 1974. Phobos: Control network analysis. *Icarus* 23, 290-299. doi: 10.1016/0019-1035(74)90007-4
Duxbury, T.C., 1991. An Analytic Model for the Phobos Surface. *Planetary and Space Science* 39, 355-376. doi: 10.1016/0032-0633(91)90157-6
Elphic, R.C., Lee, P., Zolensky, M.E., Mittlefehldt, D.W., Lim, L.F., Colaprete, A., 2016. Neutron Spectroscopy Can Constrain the Composition and Provenance of Phobos and Deimos, Lunar and Planetary Science Conference, p. 2957.
Fanale, F.P., Salvail, J.R., 1989. Loss of water from Phobos. *Geophysical Research Letters* 16, 287-290. doi: 10.1029/GL016i004p00287
Feldman, W.C., Ahola, K., Barraclough, B.L., Belian, R.D., Black, R.K., Elphic, R.C., Everett, D.T., Fuller, K.R., Kroesche, J., Lawrence, D.J., Lawson, S.L., Longmire, J.L., Maurice, S., Miller, M.C., Prettyman, T.H., Storms, S.A., Thornton, G.W., 2004. Gamma-Ray, Neutron, and Alpha-Particle Spectrometers for the Lunar Prospector mission. *Journal of Geophysical Research: Planets* 109, E07S06. doi: 10.1029/2003je002207
Fraeman, A.A., Arvidson, R.E., Murchie, S.L., Rivkin, A., Bibring, J.-P., Choo, T.H., Gondet, B., Humm, D., Kuzmin, R.O., Manaud, N., Zabalueva, E.V., 2012. Analysis of disk-resolved OMEGA and CRISM spectral observations of Phobos and Deimos. Journal of Geophysical Research 117, E00J15. doi: 10.1029/2012JE004137
Fraeman, A.A., Murchie, S.L., Arvidson, R.E., Clark, R.N., Morris, R.V., Rivkin, A.S., Vilas, F., 2014. Spectral absorptions on Phobos and Deimos in the visible/near infrared wavelengths and their compositional constraints. Icarus 229, 196-205. doi: 10.1016/j.icarus.2013.11.021
Fujimoto, M., 2017. MMX in the Context of ISAS Small Body Mission Series, PS05-13-A041. Asia Oceania Geoscience Society, Singapore.
Fujiwara, A., Asada, N., 1983. Impact fracture patterns on phobos ellipsoids. Icarus 56, 590-602. doi: 10.1016/0019-1035(83)90176-8

Futaana, Y., Barabash, S., Holmström, M., Fedorov, A., Nilsson, H., Lundin, R., Dubinin, E., Fränz, M., 2010. Backscattered solar wind protons by Phobos. Journal of Geophysical Research: Space Physics 115. doi: 10.1029/2010ja015486

Gendrin, A., Mangold, N., Bibring, J.-p., Langevin, Y., Gondet, B., Poulet, F., Bonello, G., Quantin, C., Mustard, J., Arvidson, R., LeMouélic, S., 2005. Sulfates in Martian layered terrains: the OMEGA/Mars Express view. *Science (New York, N.Y.)* 307, 1587-1591. doi: 10.1126/science.1109087

Giuranna, M., Roush, T.L., Duxbury, T., Hogan, R.C., Carli, C., Geminale, A., Formisano, V., 2011. Compositional interpretation of PFS/MEx and TES/MGS thermal infrared spectra of Phobos. *Planetary and Space Science* 59, 1308-1325. doi: 10.1016/j.pss.2011.01.019

Goldsten, J.O., Rhodes, E.A., Boynton, W.V., Feldman, W.C., Lawrence, D.J., Trombka, J.I., Smith, D.M., Evans, L.G., White, J., Madden, N.W., Berg, P.C., Murphy, G.A., Gurnee, R.S., Strohbehn, K., Williams, B.D., Schaefer, E.D., Monaco, C.A., Cork, C.P., Del Eckels, J., Miller, W.O., Burks, M.T., Hagler, L.B., DeTeresa, S.J., Witte, M.C., 2007. The MESSENGER Gamma-Ray and Neutron Spectrometer. *Space Science Reviews* 131, 339-391. doi: 10.1007/s11214-007-9262-7

Gondet, B., Bibring, J.-P., 2010. Phobos Observations by the OMEGA/Mars Express Hyperspectral Imager. EPSC 2010: The European Planetary Science Congress 5, 548.

Grebowsky, J.M., Moses, J.I., Pesnell, W.D., 2002. Meteoric Material-An Important Component of Planetary Atmospheres. *Washington DC American Geophysical Union Geophysical Monograph Series* 130, 235.

Hercík, D., Auster, H.-U., Blum, J., Fornacon, K.-H., Fujimoto, M., Gebauer, K., Güttler, C., Hillenmaier, O., Hördt, A., Liebert, E., Matsuoka, A., Nomura, R., Richter, I., Stoll, B., Weiss, B.P., Glassmeier, K.-H. 2016. The mascot Magnetometer. Space Science Reviews. doi: org/10.1007/s11214-016-0236-5

Herique A., B. Agnus, E. Asphaug, A. Barucci, P. Beck, J. Bellerose, J. Biele, L. Bonal, P. Bousquet, L. Bruzzone, C. Buck, I. Carnelli, A. Cheng, V. Ciarletti, M. Delbo, J. Du, X. Du, C. Eyraud, W. Fa, J. Gil Fernandez, O. Gassot, R. Granados-Alfaro, S.F. Green, B. Grieger, J.T. Grundmann, J. Grygorczuk, R. Hahnel, E. Heggy, T-M. Ho , O. Karatekin, Y. Kasaba , T. Kobayashi , W. Kofman, C. Krause, A. Kumamoto, M. Küppers, M. Laabs, C. Lange, J. Lasue, A.C. Levasseur- Regourd, A. Mallet, P. Michel, S. Mottola, N. Murdoch, M. Mütze, J. Oberst, R. Orosei, D. Plettemeier, S. Rochat, R. RodriguezSuquet, Y. Rogez, P. Schaffer, C. Snodgrass, J-C. Souyris, M. Tokarz, S. Ulamec, J-E. Wahlund, S. Zine, 2017, Direct Observations of Asteroid Interior and Regolith Structure: Science Measurement Requirements, ASR submitted to the same issue, in press.

Ip, W.-H., Banaszkiewicz, M., 1990. On the dust/gas tori of Phobos and Deimos. *Geophysical Research Letters* 17, 857-860. doi: 10.1029/GL017i006p00857

Ishimoto, H., Mukai, T., 1994. Phobos dust rings. *Planetary and Space Science* 42, 691-697. doi: 10.1016/0032-0633(94)90049-3

Jacobson, R.A., 2010. The Orbits and Masses of the Martian Satellites and the Libration of Phobos. *The Astronomical Journal* 139, 668-679. doi: 10.1088/0004-6256/139/2/668

Jacobson, R.A., Lainey, V., 2014. Martian satellite orbits and ephemerides. Planetary and Space Science 102, 35-44. doi: 10.1016/j.pss.2013.06.003

Jaumann, R., Neukum, G., Behnke, T., Duxbury, T.C., Eichentopf, K., Flohrer, J., Gasselt, S.v., Giese, B., Gwinner, K., Hauber, E., Hoffmann, H., Hoffmeister, A., Köhler, U., Matz, K.-D., McCord, T.B., Mertens, V., Oberst, J., Pischel, R., Reiss, D., Ress, E., Roatsch, T., Saiger, P., Scholten, F., Schwarz, G., Stephan, K., Wählisch, M., 2007. The high-resolution stereo camera (HRSC) experiment on Mars Express: Instrument aspects and experiment conduct from interplanetary cruise through the nominal mission. *Planetary and Space Science* 55, 928-952. doi: 10.1016/j.pss.2006.12.003

Juhász, A., Horányi, M., 1995. Dust torus around Mars. *Journal of Geophysical Research* 100, 3277. doi: 10.1029/94JE03044

Kholshevnikov, K.V., Krivov, A.V., Sokolov, L.L., Titov, V.B., 1993. The dust torus around PHOBOS orbit. *Icarus* 105, 351. doi: 10.1006/icar.1993.1132

Krivov, A.V., Feofilov, A.G., Dikarev, V.V., 2006. Search for the putative dust belts of Mars: The late 2007 opportunity. *Planetary and Space Science* 54, 871-878. doi: 10.1016/j.pss.2006.05.007

Krivov, A.V., Hamilton, D.P., 1997. Martian Dust Belts: Waiting for Discovery. *Icarus* 128, 335-353. doi: 10.1006/icar.1997.5753

Kuramoto, K., Kawakatsu, Y., Fujimoto, M., Team, M.S., 2017. Martian Moons Exploration (MMX) Conceptual Study Results, Lunar and Planetary Science Conference.

Lainey, V., Dehant, V., Pätzold, M., 2007. First numerical ephemerides of the Martian moons. *Astronomy & Astrophysics* 465, 1075-1084. doi: 10.1051/0004-6361:20065466

Lainey, V., Pasewaldt, A., Robert, V., Rosenblatt, P., Andert, T., Pätzold, M., Thuillot, W., 2016. Mars moon ephemerides after Mars Express 2013 flyby. *Astronomy & Astrophysics*, Under Review.

Lawrence, D.J., Feldman, W.C., Goldsten, J.O., Maurice, S., Peplowski, P.N., Anderson, B.J., Bazell, D., McNutt, R.L., Nittler, L.R., Prettyman, T.H., Rodgers, D.J., Solomon, S.C., Weider, S.Z., 2013. Evidence for Water Ice Near Mercury's North Pole from MESSENGER Neutron Spectrometer Measurements. *Science* 339, 292-296. doi: 10.1126/science.1229953

Longobardo, A., Palomba, E., De Sanctis, M.C., Zinzi, A., Scully, J.E.C., Capaccioni, F., Tosi, F., Zambon, F., Ammannito, E., Combe, J.-P., Raymond, C.A., Russell, C.T., 2015. Mineralogical and spectral analysis of Vesta's Gegania and Lucaria quadrangles and comparative analysis of their key features. ICARUS 259, 72-90. doi: http://dx.doi.org/10.1016/j.icarus.2015.04.031

Michel, P., Cheng, A., Küppers, M., Pravec, P., Blum, J., Delbo, M., Green, S.F., Rosenblatt, P., Tsiganis, K., Vincent, J.B., Biele, J., Ciarletti, V., Hérique, A., Ulamec, S., Carnelli, I., Galvez, A., Benner, L., Naidu, S.P., Barnouin, O.S., Richardson, D.C., Rivkin, A., Scheirich, P., Moskovitz, N., Thirouin, A., Schwartz, S.R., Campo Bagatin, A., Yu, Y., 2016. Science case for the Asteroid Impact Mission (AIM): A component of the Asteroid Impact & Deflection Assessment (AIDA) mission. Advances in Space Research 57, 2529–2547. doi:10.1016/j.asr.2016.03.031

Molina-Cuberos, G.J., Witasse, O., Lebreton, J.-P., Rodrigo, R., López-Moreno, J.J., 2003. Meteoric ions in the atmosphere of Mars. *Planetary and Space Science* 51, 239-249. doi: 10.1016/S0032-0633(02)00197-6

Mottola, S., Arnold, G., Grothues, H.-G., Jaumann, R., Michaelis, H., Neukum, G., Bibring, J.-P., 2007. The Rolis Experiment on the Rosetta Lander. *Space Science Reviews* 128, 241-255. doi: 10.1007/s11214-006-9004-2

Murchie, S.L., Britt, D.T., Head, J.W., Pratt, S.F., Fisher, P.C., 1991. Color heterogeneity of the surface of Phobos - Relationships to geologic features and comparison to meteorite analogs. *Journal of Geophysical Research* 96, 5925-5945. doi: 10.1029/90JB02354

Murchie, S.L., Britt, D.T., Pieters, C.M., 2014. The value of Phobos sample return. *Planetary and Space Science* 102, 176-182. doi: 10.1016/j.pss.2014.04.014

Murchie, S.L., Choo, T., Humm, D., Rivkin, A.S., Bibring, J.-P., Langevin, Y., Gondet, B., Roush, T.L., Duxbury, T., Team, C., 2008. MRO/CRISM Observations of Phobos and Deimos, Lunar and Planetary Science Conference, p. 1434.

Murchie, S., Erard, S., 1996. Spectral Properties and Heterogeneity of Phobos from Measurements byPhobos 2. *Icarus* 123, 63-86. doi: 10.1006/icar.1996.0142

Murchie, S.L., Thomas, P.C., Rivkin, A.S., Chabot, N.L., 2015. Phobos and Deimos, in: Michel, P., DeMeo, F.E., Bottke, W.F. (Eds.), Asteroids IV, pp. 451-467.

Murray, J.B., Heggie, D.C., 2014. Character and origin of Phobos' grooves. *Planetary and Space Science* 102, 119-143. doi: 10.1016/j.pss.2014.03.001

Murray, J.B., Iliffe, J.C., 2011. Morphological and geographical evidence for the origin of Phobos' grooves from HRSC Mars Express images. *Geological Society, London, Special Publications* 356, 21-41. doi: 10.1144/SP356.3

Oberst, J., Schwarz, G., Behnke, T., Hoffmann, H., Matz, K.D., Flohrer, J., Hirsch, H., Roatsch, T., Scholten, F., Hauber, E., Brinkmann, B., Jaumann, R., Williams, D., Kirk, R., Duxbury, T., Leu, C., Neukum, G., 2008. The imaging performance of the SRC on Mars Express. *Planetary and Space Science* 56, 473-491. doi: 10.1016/j.pss.2007.09.009

Oberst, J., Zubarev, A., Nadezhdina, I., Shishkina, L., Rambaux, N., 2014. The Phobos geodetic control point network and rotation model. *Planetary and Space Science* 102, 45-50. doi: 10.1016/j.pss.2014.03.006

Øieroset, M., Brain, D.A., Simpson, E., Mitchell, D.L., Phan, T.D., Halekas, J.S., Lin, R.P., Acuña, M.H., 2010. Search for Phobos and Deimos gas/dust tori using in situ observations from Mars Global Surveyor MAG/ER. *Icarus* 206, 189-198. doi: 10.1016/j.icarus.2009.07.017

Paral, J., Trávníček, P.M., Rankin, R., Schriver, D., 2010. Sodium ion exosphere of Mercury during MESSENGER flybys. *Geophysical Research Letters* 37. doi: 10.1029/2010gl044413

Pätzold, M., Andert, T., Jacobson, R., Rosenblatt, P., Dehant, V., 2014a. Phobos: Observed bulk properties. *Planetary and Space Science* 102, 86-94. doi: 10.1016/j.pss.2014.01.004

Pätzold, M., Andert, T.P., Asmar, S.W., Anderson, J.D., Barriot, J.-P., Bird, M.K., Häusler, B., Hahn, M., Tellmann, S., Sierks, H., Lamy, P., Weiss, B.P., 2011. Asteroid 21 Lutetia: low mass, high density. *Science (New York, N.Y.)* 334, 491-492. doi: 10.1126/science.1209389

Pätzold, M., Andert, T.P., Tyler, G.L., Asmar, S.W., Häusler, B., Tellmann, S., 2014b. Phobos mass determination from the very close flyby of Mars Express in 2010. *Icarus* 229, 92-98. doi: 10.1016/j.icarus.2013.10.021

Peplowski, P.N., Bazell, D., Evans, L.G., Goldsten, J.O., Lawrence, D.J., Nittler, L.R., 2015. Hydrogen and major element concentrations on 433 Eros: Evidence for an L- or LL-chondrite-like surface composition. Meteoritics & Planetary Science 50, 353-367. doi: 10.1111/maps.12434

Peplowski, P.N., Lawrence, D.J., Rhodes, E.A., Sprague, A.L., McCoy, T.J., Denevi, B.W., Evans, L.G., Head, J.W., Nittler, L.R., Solomon, S.C., Stockstill-Cahill, K.R., Weider, S.Z., 2012. Variations in the abundances of potassium and thorium on the surface of Mercury: Results from the MESSENGER Gamma-Ray Spectrometer. *Journal of Geophysical Research: Planets* 117. doi: 10.1029/2012je004141

Picardi, G., Biccari, D., Seu, R., Marinangeli, L., Johnson, W.T.K., Jordan, R.L., Plaut, J., Safaenili, A., Gurnett, D.a., Ori, G.G., Orosei, R., Calabrese, D., Zampolini, E., 2004. Performance and surface scattering models for the Mars Advanced Radar for Subsurface and Ionosphere Sounding (MARSIS). *Planetary and Space Science* 52, 149-156. doi: 10.1016/j.pss.2003.08.020

Pieters, C.M., Murchie, S., Thomas, N., Britt, D., 2014. Composition of Surface Materials on the Moons of Mars. Planetary and Space Science 102, 144-151. doi: 10.1016/j.pss.2014.02.008

Pieters, C.M., Taylor, L.A., Noble, S.K., Keller, L.P., Hapke, B., Morris, R.V., Allen, C.C., McKay, D.S., Wentworth, S., 2000. Space weathering on airless bodies: Resolving a mystery with lunar samples. Meteoritics and Planetary Science 35, 1101-1107. doi: 10.1111/j.1945-5100.2000.tb01496.x

Plettemeier, D., Hahnel, R., Hegler, S., Safaeinili, A., Orosei, R., Cicchetti, A., Plaut, J., Picardi, G., 2009. Simulation of Radar-Backscattering from Phobos - A Contribution to the Experiment MARSIS aboard MarsExpress, in: Arabelos, D.N., Tscherning, C.C. (Eds.), EGU General Assembly Conference Abstracts, p. 3763.

Poppe, A.R., Curry, S.M., Fatemi, S., McFadden, J.P., Delory, G.T., 2015. Modeling the Phobos and Deimos Neutral Gas Tori: Implications for Detection by MAVEN, Lunar and Planetary Science Conference, p. 1399.

Ramsley, K.R., Head, J.W., 2013a. Mars impact ejecta in the regolith of Phobos: Bulk concentration and distribution. *Planetary and Space Science* 87, 115-129. doi: 10.1016/j.pss.2013.09.005

Ramsley, K.R., Head, J.W., 2013b. The origin of Phobos grooves from ejecta launched from impact craters on Mars: Tests of the hypothesis. *Planetary and Space Science* 75, 69-95. doi: 10.1016/j.pss.2012.10.007

Rivkin, A.S., Brown, R.H., Trilling, D.E., Bell III, J.F., Plassmann, J.H., 2002. Near-Infrared Spectrophotometry of Phobos and Deimos. *Icarus* 156, 64-75. doi: 10.1006/icar.2001.6767

Rosenblatt, P., 2011. The origin of the Martian moons revisited. *The Astronomy and Astrophysics Review* 19, 44. doi: 10.1007/s00159-011-0044-6

Rosenblatt, P., Charnoz, S., 2012. On the formation of the martian moons from a circum-martian accretion disk. *Icarus* 221, 806-815. doi: 10.1016/j.icarus.2012.09.009

Rosenblatt, P., Charnoz, S., Dunseath, K.M., Terao-Dunseath, M., Trinh, A., Hyodo, R., Genda, H., Toupin, S., 2016. Accretion of Phobos and Deimos in an extended debris disc stirred by transient moons. *Nature Geosci* 9, 581-583. doi: 10.1038/ngeo2742

Rosenblatt, P., Lainey, V., Le Maistre, S., Marty, J.C., Dehant, V., Pätzold, M., van Hoolst, T., Häusler, B., 2008. Accurate Mars Express orbits to improve the determination of the mass and ephemeris of the Martian moons. *Planetary and Space Science* 56, 1043-1053. doi: 10.1016/j.pss.2008.02.004

Rosenblatt, P., Rambaux, N., Le Maistre, S., 2009. The interior structure of Phobos, Brown-Vernadsky micro-symposium.

Rubincam, D.P., Chao, B.F., Thomas, P.C., 1995. The Gravitational Field of Deimos. ICARUS 114, 63-67. doi: http://dx.doi.org/10.1006/icar.1995.1043

Safronov, V.S., Vitjazev, A.V., 1986. The Origin and Early Evolution of the Terrestrial Planets, in: Saxena, S.K. (Ed.), Chemistry and Physics of Terrestrial Planets. Springer New York, New York, NY, pp. 1-29.

Saito, Y., Yokota, S., Tanaka, T., Asamura, K., Nishino, M.N., Fujimoto, M., Tsunakawa, H., Shibuya, H., Matsushima, M., Shimizu, H., Takahashi, F., Mukai, T., Terasawa, T., 2008. Solar wind proton reflection at the lunar surface: Low energy ion measurement by MAP-PACE onboard SELENE (KAGUYA). Geophysical Research Letters 35, L24205. doi: 10.1029/2008GL036077

Scully, J.E.C., Yin, A., Russell, C.T., Buczkowski, D.L., Williams, D.A., Blewett, D.T., Ruesch, O., Hiesinger, H., Le Corre, L., Mercer, C., Yingst, R.A., Garry, W.B., Jaumann, R., Roatsch, T., Preusker, F., Gaskell, R.W., Schröder, S.E., Ammannito, E., Pieters, C.M., Raymond, C.A., 2014. Geomorphology and structural geology of Saturnalia Fossae and adjacent structures in the northern hemisphere of Vesta. ICARUS 244, 23-40. doi: http://dx.doi.org/10.1016/j.icarus.2014.01.013

Shi, X., Willner, K., Oberst, J., Ping, J., Ye, S., 2012. Working models for the gravitational field of Phobos. *Science China Physics, Mechanics and Astronomy* 55, 358-364. doi: 10.1007/s11433-011-4606-4

Sierks, H., Keller, H.U., Jaumann, R., Michalik, H., Behnke, T., Bubenhagen, F., Büttner, I., Carsenty, U., Christensen, U., Enge, R., Fiethe, B., Gutiérrez Marqués, P., Hartwig, H., Krüger, H., Kühne, W., Maue, T., Mottola, S., Nathues, A., Reiche, K.-U., Richards, M.L., Roatsch, T., Schröder, S.E., Szemerey, I., Tschentscher, M., 2011. The Dawn Framing Camera. *Space Science Reviews* 163, 263-327. doi: 10.1007/s11214-011-9745-4

Simonelli, D.P., Thomas, P.C., Carcich, B.T., Veverka, J., 1993. The Generation and Use of Numerical Shape Models for Irregular Solar System Objects. *ICARUS* 103, 49-61. doi: 10.1006/icar.1993.1057

Soter, S., 1971. The Dust Belts of Mars. CRSR Rept. No. 462, Cornell University

Stickle, A.M., Schultz, P.H., Crawford, D.A., 2015. Subsurface failure in spherical bodies: A formation scenario for linear troughs on Vesta's surface. *Icarus* 247, 18-34. doi: 10.1016/j.icarus.2014.10.002

Thomas, N., Stelter, R., Ivanov, A., Bridges, N.T., Herkenhoff, K.E., McEwen, A.S., 2011. Spectral heterogeneity on Phobos and Deimos: HiRISE observations and comparisons to Mars Pathfinder results. *Planetary and Space Science* 59, 1281-1292. doi: 10.1016/j.pss.2010.04.018

Thomas, P.C., 1989. The shapes of small satellites. *Icarus* 77, 248-274. doi: 10.1016/0019-1035(89)90089-4

Thomas, P.C., 1993. Gravity, Tides, and Topography on Small Satellites and Asteroids: Application to Surface Features of the Martian Satellites. *Icarus* 105, 326-344. doi: 10.1006/icar.1993.1130

Thomas, P.C., Adinolfi, D., Helfenstein, P., Simonelli, D., Veverka, J., 1996. The Surface of Deimos: Contribution of Materials and Processes to Its Unique Appearance. *Icarus* 123, 536-556. doi: 10.1006/icar.1996.0177

Thomas, P., Veverka, J., Bell, J., Lunine, J., Cruikshank, D., 1992. Satellites of Mars - Geologic history. In: Mars (A93-27852 09-91), pp. 1257-1282.

Thomas, P.C., Veverka, J., Sullivan, R., Simonelli, D.P., Malin, M.C., Caplinger, M., Hartmann, W.K., James, P.B., 2000. Phobos: Regolith and ejecta blocks investigated with Mars Orbiter Camera images. *Journal of Geophysical Research: Planets* 105, 15091-15106. doi: 10.1029/1999je001204

Turner, R.J., 1978. A Model of Phobos. *International Journal of Solar System Studies* 33, 116-140. doi: 10.1016/0019-1035(78)90028-3

Veselovsky, I.S., 2004. Is Phobos Magnetized? Solar System Research 38, 188-193. doi: 10.1023/B:SOLS.0000030858.10477.6c

Wieser, M., Barabash, S., 2016. A family for miniature, easily reconfigurable particle sensors for space plasma measurements. *Journal of Geophysical Research: Space Physics* 121, 11,588-511,604. doi: 10.1002/2016ja022799

Wieser, M., Barabash, S., Futaana, Y., Holmström, M., Bhardwaj, A., Sridharan, R., Dhanya, M.B., Wurz, P., Schaufelberger, A., Asamura, K., 2009. Extremely high reflection of solar wind protons as neutral hydrogen atoms from regolith in space. *Planetary and Space Science* 57, 2132-2134. doi: 10.1016/j.pss.2009.09.012

Willner, K., 2009. The Martian Moon Phobos - A Geodetic Analysis of its Motion, Orientation, Shape, and Physical Parameters, doctoral, Technische Universität Berlin. 10.14279/depositonce-2338

Willner, K., Oberst, J., Hussmann, H., Giese, B., Hoffmann, H., Matz, K.-D., Roatsch, T., Duxbury, T., 2010. Phobos control point network, rotation, and shape. *Earth and Planetary Science Letters* 294, 541-546. doi: 10.1016/j.epsl.2009.07.033

Willner, K., Shi, X., Oberst, J., 2014. Phobos' shape and topography models. *Planetary and Space Science* 102, 51-59. doi: 10.1016/j.pss.2013.12.006

Zakharov, A., Horanyi, M., Lee, P., Witasse, O., Cipriani, F., 2014. Dust at the Martian moons and in the circummartian space. *Planetary and Space Science* 102, 171-175. doi: 10.1016/j.pss.2013.12.011